A weak-inertia mathematical model of bubble growth in a polymer foam

Journal of Non-Newtonian Fluid Mechanics 244 (2017) 1–14

Contents lists available at ScienceDirect

Journal of Non-Newtonian Fluid Mechanics

journal homepage: www.elsevier.com/locate/jnnfm

A weak-inertia mathematical model of bubble growth in a polymer foam

Euan Barlow[a,b,*], Aoibhinn M. Bradley[a], Anthony J. Mulholland[a], Carmen Torres-Sanchez[c]

[a] Department of Mathematics and Statistics, University of Strathclyde, Glasgow, G1 1XH, UK
[b] Department of Management Science, University of Strathclyde, Glasgow, G4 0GE, UK
[c] Wolfson School of Mechanical, Electrical and Manufacturing Engineering, Loughborough University, Loughborough, LE11 3TU, UK

ARTICLE INFO

Article history:
Received 23 July 2016
Accepted 31 March 2017
Available online 5 April 2017

Keywords:
Bubble growth
Polymeric foam
Oldroyd-B fluid
Analytic solution
Inertia

ABSTRACT

One possible manufacturing method for bone scaffolds used in regenerative medicine involves the acoustic irradiation of a reacting polymer foam to generate a graded porosity. This paper derives a mathematical model of a non-reacting process in order to develop theoretical confirmation of the influence of the acoustic signal on the polymer foam. The model describes single bubble growth in a free rising, non-reacting polymer foam irradiated by an acoustic standing wave and incorporates the effects of inertia. Leading and first order asymptotic inner solutions in the temporal domain (early growth) are presented for the case of instantaneous diffusion when the fluid volume surrounding the bubble is large compared to the bubble volume. The leading order asymptotic outer solution (late growth), for the case of instantaneous diffusion, is described analytically using the Picard iteration method. Initial conditions for this outer solution are identified through matching with the asymptotic inner solution. A numerical solution for the leading order outer equation is also presented. Investigations are carried out to explore the influence of inertia on the bubble volume, fluid pressure and the stress tensors of the foam, and to explore the effect of fluid viscosity and acoustic pressure amplitude on the final bubble volume, and the curing time. A key result is that increasing the applied acoustic pressure is shown to result in a reduced steady state bubble volume, indicating that ultrasonic irradiation has the potential to produce tailored porosity profiles in bioengineering scaffolds.

1. Introduction

1.1. Motivation

A polymeric foam is a particular example of a viscoelastic, heterogeneous material which is composed of at least two phases (one solid plus voids whose size distribution can be varied [43]). Bone scaffolds [43] are the biocompatible materials which provide the support structure for the growth of tissue engineered bone precursors [8,20]. The physical properties of polymeric foams make these particularly suitable for bone scaffold applications, including their low density, chemical inertness, high wear resistance, biodegradability and thermal and acoustic insulation. One of the factors contributing to the strength and functionality of natural bone is its functionally graded porosity, with higher density on the periphery of the structure and higher porosity at the centre [6]. The best grafts and bone substitutes are considered to be those with biomechanical and biological properties most closely resembling the non-uniform graded porosity distribution observed in natural bone [6], and it is therefore desirable to mimic this property.

A number of different approaches to the tailored design and manufacture of bone scaffolds have been reported, including control of the processing conditions and of the chemical composition of the polymer material [9,40,48]. Ultrasonic irradiation of liquids has been shown experimentally to result in a number of unusual phenomena including rectified diffusion and increased polymerisation reaction rate [19,22,32,42]. Torres-Sanchez and Corney [43] developed an empirical method for designing bone scaffolds, which uses an acoustic standing wave to irradiate a sample of polymerising polyurethane foam to tailor the porosity profile within the final cured sample to a particular porosity specification. A relationship between the pressure amplitude of the irradiating sound wave and the porosity value at a given position in the sam-

* Corresponding author:
E-mail address: euan.barlow@strath.ac.uk (E. Barlow).

http://dx.doi.org/10.1016/j.jnnfm.2017.03.008

ple was demonstrated experimentally. Ultrasound was observed to have an impact at particular stages during the reaction, and the authors hypothesized that this was due to the fact that diffusion and convection were predominant effects during these stages.

This paper presents the first attempt at mathematically modelling the experiment presented by Torres Sanchez and Corney [43] and the key mechanisms involved in this complex reaction, to develop an understanding of this process and provide the first steps towards supporting the production of strictly defined and controlled porosity profiles. Polymerisation is a complex process involving factors such as bubble dynamics, evolving rheology [16,28], a two-phase fluid, rectified diffusion [10–13,25], Bjerknes forces [3,23] and Ostwald ripening [27,35]. Of additional relevance in this study is the effect of the ultrasonic irradiation. To make headway with modelling this complex process, concentration is focused on the post nucleation evolution of a bubble in a viscoelastic fluid and the effects of rectified diffusion, Bjerknes forces and Ostwald ripening are ignored. The effect of the ultrasound pressure amplitude on the long term growth of the bubble is, however, considered. The effects of inertia are incorporated into the model as it plays a significant role in the early stages of the bubble's evolution.

1.2. Bubble dynamics

Much work has been done to study and model the nucleation [18,36,38] and subsequent single bubble growth [5,14–18,30,37–39,41,45] in viscoelastic materials including polymer foams, both reacting [16] and non-reacting [14–17,49]. The effects of ultrasound on nucleation [50] and subsequent growth of a single bubble via rectified diffusion in an aqueous fluid [24,26,29,33,34] have been studied extensively.

There have been a number of studies of the nucleation and subsequent growth of a single spherical gas bubble in a surrounding fluid due to diffusion of gas through the fluid and into the bubble. Amon and Denson [4] proposed a cell model for the analysis of bubble growth in an expanding polymer foam with each cell containing a spherical gas bubble surrounded by a concentric liquid envelope containing a limited supply of gas. Their model takes account of heat transfer and inertia and couples bubble growth to the changing foam density. Street et al. [39] and Ting [41] both used the Oldroyd B fluid model to describe the viscoelasticity of the surrounding fluid layer which they assumed to be infinite. This resembles the case of early time foaming where bubble size is small and bubbles are spaced at large distances from each other, remaining spherical and not interfering with each other. They demonstrated that the viscoelasticity of the melt as well as the diffusivity of the gas determined the initial growth rate. Arefmanesh and Advani [5] considered the case of a spherical gas bubble surrounded by a finite shell of viscoelastic fluid which they modelled using the upper convected Maxwell model. They introduced a Lagrangian transformation to describe the moving bubble/liquid interface and substituted a concentration potential to aid numerical solution. Their model serves to describe the case where a large number of bubbles exist in close proximity to each other, which can be expected in an expanding polymer foam. Shafi and co-workers [36,37] looked at bubble growth in polymer foams in conjunction with nucleation and concluded that the most sensitive parameters to final bubble size distribution are those associated with nucleation. They found that while growth dynamics can alter the distribution this is only a secondary effect. Feng and Bertelo [18] also looked at the effect of nucleation but proposed a model for heterogeneous nucleation and its effect on the final bubble size distribution. Venerus et al. [45] formulate a model of diffusion induced bubble growth in viscoelastic liquids of infinite extent, demonstrating that under various approximations, several previously published models can be derived from their model, and providing comparison between models. In Venerus [44], transport models of diffusion induced bubble growth in viscous liquids of both finite and infinite extent are developed and evaluated, and results compared with Amon and Denson [4] and Arefmanesh and Advani [5]. Both models agree at early stages of the growth process and differ at later stages when the equilibrium bubble radius is approached for the finite liquid model.

Building on the above work, Everitt et al. [16] proposed two models for individual bubble expansion in curing polymer foams. The first model was for bubble growth in a non-reacting polymer foam; the second models the gas production due to the reaction and the evolving rheology of the viscoelastic material in the reacting polymer foam. In each case the evolving fluid is treated as a multimode Oldroyd B system, and the Lagrangian transformation is used to describe the moving bubble boundary. Everitt et al. [16] neglected the effects of inertia since nondimensionalisation of their system results in a very small Reynolds number, and their model does not include an acoustic forcing term.

1.3. Overview

This paper examines the effect of ultrasonic irradiation on the dynamics of a single bubble in an expanding polymer foam. The non-reacting model proposed by Everitt et al. [16] is extended to include the effects of inertia and the effects of a standing acoustic wave sonicating the polymerising sample. The model equations are derived by consideration of an Oldroyd B polymeric fluid [46]. Once the governing equations, initial and boundary conditions are obtained, an instantaneous diffusion assumption is made in order to partially decouple the system. This is then probed in an effort to derive an approximate analytic solution using asymptotic expansions for the case where the bubble volume is much smaller than the surrounding fluid volume. This regime may describe the situation at early time in the polymerising sample when bubbles have just nucleated and are at large distances from each other so that they are effectively surrounded by an infinite fluid volume. An inner and outer asymptotic solution are proposed; the former to first order and the latter to leading order. The accuracy of the first order asymptotic inner solution is discussed before a leading order analytic solution for the outer temporal variable is derived, where the initial conditions for this outer solution are generated through matching with the asymptotic expansion of the inner solution. A numerical scheme is produced to test the accuracy of the analytic outer solution and the limitations of the analytic solution are discussed before using the numerical scheme to predict the effects of changing viscosity and acoustic pressure amplitude on the outer solution.

Section 2 presents the derivation of the model of bubble growth in a free rising, non-reacting polymer foam irradiated by an acoustic standing wave and incorporating the effects of inertia. The asymptotic derivation of the inner and outer solutions are given in Sections 3 and 4, respectively. Concluding remarks and areas of future work are discussed in Section 5.

2. Mathematical model of a non-reacting foam

In the non-reacting case a polymeric liquid containing a foaming agent is subjected to a sudden reduction in pressure and foaming commences as the foaming agent comes out of solution [16]. This is a two phase system with the foam considered to be a system of identical, spherical bubbles of gas, each surrounded by a layer of viscoelastic fluid containing a quantity of dissolved gas. The model concerns a single bubble with initial volume, $4\pi u(0)/3 = 4\pi R^3/3$, with bubble radius R and initial gas pressure p_{g0}. The fluid surrounding the bubble is assumed to be

incompressible, viscoelastic and containing a limited supply of dissolved ideal gas. The initial bubble volume is the volume when the bubble gas pressure is p_{g0} and is larger than the nucleation volume. It is further assumed that the bubble undergoes spherically symmetric expansion driven by the pressure difference across the bubble-fluid interface, $(p_{g0} - p_a)$, where p_a is the ambient gas pressure (the atmospheric pressure combined with the hydrostatic pressure). The conditions are isothermal and the bubble-fluid interface is in thermodynamic equilibrium [16]. First, the dynamics of the fluid layer are considered; the system is modelled using the Oldroyd B system of equations for a viscoelastic medium [46]. Subsequently, the gaseous phase, its concentration in, and diffusion through, the fluid, and its transport across the bubble-fluid interface are modelled.

A solution of polymer molecules in a Newtonian liquid exhibits both viscous and elastic behaviour [47] and can be modelled as an Oldroyd B fluid [46]. The derivation below follows closely that in [16] but here inertia is included, and so only the key equations are presented. The general governing equations of this fluid are

$$\nabla \cdot \mathbf{q} = 0, \tag{2.1}$$

$$-p\mathbf{I} + \mu\left(\nabla\mathbf{q} + (\nabla\mathbf{q})^T\right) + G(\mathbf{A} - \mathbf{I}) = \boldsymbol{\sigma}, \tag{2.2}$$

$$\rho\left(\frac{\partial \mathbf{q}}{\partial t} + \mathbf{q}\cdot\nabla\mathbf{q}\right) = \nabla\cdot\boldsymbol{\sigma}, \tag{2.3}$$

$$\frac{\partial \mathbf{A}}{\partial t} + (\mathbf{q}\cdot\nabla)\mathbf{A} - \mathbf{A}\cdot\nabla\mathbf{q} - (\nabla\mathbf{q})^T\cdot\mathbf{A} = -\frac{1}{\tau}(\mathbf{A} - \mathbf{I}), \tag{2.4}$$

where $\mathbf{q}$ is the velocity vector, $\boldsymbol{\sigma}$ is the stress tensor, μ is the solvent viscosity, ρ is the fluid density, G is the relaxation modulus associated with the polymer stress, $\mathbf{A}$ the orientation tensor, $\mathbf{I}$ the identity matrix and τ represents the relaxation time of a polymer molecule.

The bubble expansion is assumed to be spherically symmetric so that only the radial component of the velocity vector is non-zero, and is dependent on the radial co-ordinate, r (with origin at the bubble centre), and time t. The continuity Eq. (2.1) then solves to give

$$\mathbf{q} = \frac{\dot{R}R^2}{r^2}\mathbf{e}_r. \tag{2.5}$$

The gradient of this first order Cartesian tensor [21] is evaluated as

$$\nabla\mathbf{q} = \frac{\dot{R}R^2}{r^3}\begin{pmatrix} -2 & 0 & 0 \\ 0 & 1 & 0 \\ 0 & 0 & 1 \end{pmatrix}. \tag{2.6}$$

For spherically symmetric expansion all the off-diagonal components of the orientation tensor $\mathbf{A}$ are equal to zero and $A_{\theta\theta} = A_{\phi\phi}$. Therefore, the only non-zero components of the stress tensor $\boldsymbol{\sigma}$ are, by Eq. (2.2),

$$\sigma_{rr} = -p - 4\mu\frac{\dot{R}R^2}{r^3} + GA_{rr}, \tag{2.7}$$

$$\sigma_{\theta\theta} = -p + 2\mu\frac{\dot{R}R^2}{r^3} + GA_{\theta\theta}, \tag{2.8}$$

and

$$\sigma_{\phi\phi} = \sigma_{\theta\theta}.$$

In spherical polar co-ordinates and with spherically symmetric expansion, only the radial component of the divergence of the second order Cartesian tensor $\boldsymbol{\sigma}$ [21] is non-zero. Substituting Eqs. (2.7) and (2.8) into the right hand side of the momentum Eq. (2.3), and using Eqs. (2.5) and (2.6) to expand the inertia term on the left hand side, Eq. (2.3) can then be stated as

$$\rho\left(\frac{\ddot{R}R^2 + 2R\dot{R}^2}{r^2} - \frac{2\dot{R}^2R^4}{r^5}\right) = -\frac{\partial p}{\partial r} + G\frac{\partial A_{rr}}{\partial r} + \frac{2G}{r}(A_{rr} - A_{\theta\theta}). \tag{2.9}$$

The boundary conditions require continuity of stress to be applied at the inner and outer fluid boundaries. In the current co-ordinate system the bubble-fluid interface and the outer fluid layer are each moving with time, and the respective boundary conditions would therefore require updating through time. With conservation of the fluid volume, the system can be transformed to the Lagrangian volume co-ordinate system to simplify the analyses, where the frame of reference moves with the bubble-fluid interface [16]. Due to the spherically symmetric expansion only the radial co-ordinate requires consideration in the analysis.

Letting the conserved fluid volume equal $4\pi X/3$, the governing equations and variables can then be restated using the general fluid volume variable x, which ranges from $x = 0$ at the bubble surface to $x = X$ at the outer fluid volume limit. By defining the general bubble volume, $u(t)$, as $4\pi u(t)/3 = 4\pi R(t)^3/3$, then at a generic volume co-ordinate $4\pi u/3 + 4\pi x/3$ the associated radial position in the fluid relative to the origin at the centre of the bubble is given as $r = (u + x)^{\frac{1}{3}}$, and the radial variables R and r can therefore be replaced with the volumetric variables u and x. Eq. (2.9) can then be transformed to the Lagrangian volume co-ordinate, x, which leads to

$$\rho\left[-\frac{\ddot{u}}{3(x+u)^{\frac{1}{3}}} + \frac{\dot{u}^2}{18(x+u)^{\frac{4}{3}}}\right] = -p(x) + GA_{rr} + \frac{2}{3}G\int^x \frac{(A_{rr} - A_{\theta\theta})}{(x'+u)}dx' + C_1, \tag{2.10}$$

where C_1 is an arbitrary constant of integration to be determined by application of the boundary conditions, which are derived by considering the stresses acting on each boundary. The stresses within the fluid at each boundary are a combination of the isotropic pressure, Newtonian stress and polymer stress. At the bubble/fluid interface these fluid stresses are balanced by the bubble pressure and surface tension, whereas at the outer fluid surface the fluid stresses are balanced by the ambient pressure and the ultrasound pressure excitation.

This results in the following two boundary conditions, at $x = 0$ and $x = X$, in the Lagrangian frame,

$$-p(0) - \frac{4\mu\dot{u}}{3u} + GA_{rr}(0) = -p_g + \frac{2S}{u^{\frac{1}{3}}}, \qquad \text{at } x = 0, \tag{2.11}$$

$$-p(X) - \frac{4\mu\dot{u}}{3(X+u)} + GA_{rr}(X) = -p_a - p_u, \qquad \text{at } x = X, \tag{2.12}$$

where S is the surface tension, p_g is the bubble gas pressure, X is the Lagrangian volume co-ordinate for the outer fluid boundary and p_u is the pressure amplitude of the applied ultrasound signal. The wavelength of the applied ultrasound signal is assumed to be substantially longer than the bubble size, so that the pressure field does not impose a spatial gradient on the bubble and the assumption of spherically symmetric bubble expansion remains valid.

Evaluating (2.10) at $x = 0$ and $x = X$, and substituting from boundary conditions (2.11) and (2.12), the momentum equation can be written as

$$\frac{4}{3}\mu\dot{u}\left(\frac{1}{u} - \frac{1}{X+u}\right) + \rho\left[\frac{\ddot{u}}{3}\left(\frac{1}{u^{\frac{1}{3}}} - \frac{1}{(X+u)^{\frac{1}{3}}}\right) - \frac{\dot{u}^2}{18}\left(\frac{1}{u^{\frac{4}{3}}} - \frac{1}{(X+u)^{\frac{4}{3}}}\right)\right]$$

$$= p_g - p_a - p_u + \frac{2}{3}G\int_0^X \frac{(A_{rr}-A_{\theta\theta})}{(x'+u)}dx' - \frac{2S}{u^{\frac{1}{3}}}. \tag{2.13}$$

The only remaining unknown in the Oldroyd B system (2.1)–(2.4) is the orientation tensor $\mathbf{A}$ which is described by (2.4). In the Lagrangian frame the convection term $(\mathbf{q}\cdot\nabla)\mathbf{A}$ is zero, and (2.4) reduces to

$$\frac{\partial \mathbf{A}}{\partial t} = \mathbf{A}\cdot\nabla\mathbf{q} + (\nabla\mathbf{q})^T\cdot\mathbf{A} - \frac{1}{\tau}(\mathbf{A}-\mathbf{I}).$$

Substitution for $\nabla\mathbf{q}$ from (2.6) gives the evolution equations for A_{rr} and $A_{\theta\theta}$ as [16]

$$\frac{\partial A_{rr}}{\partial t} = -\frac{4\dot{u}}{3(u+x)}A_{rr} - \frac{1}{\tau}(A_{rr}-1), \tag{2.14}$$

and

$$\frac{\partial A_{\theta\theta}}{\partial t} = \frac{2\dot{u}}{3(u+x)}A_{\theta\theta} - \frac{1}{\tau}(A_{\theta\theta}-1). \tag{2.15}$$

Subtracting (2.14) from (2.15) gives the first normal difference rate equation

$$\frac{\partial (A_{rr}-A_{\theta\theta})}{\partial t} = \frac{2\dot{u}}{3(u+x)}[(A_{rr}-A_{\theta\theta}) - 3A_{rr}] - \frac{1}{\tau}(A_{rr}-A_{\theta\theta}), \tag{2.16}$$

where the initial conditions are given by $A_{rr} = A_{\theta\theta} = 1$ everywhere at $t = 0$.

The dissolved gas concentration contained in the fluid, $c(x, t)$, is governed by the convection-diffusion equation [49], which is derived from the assumption of mass conservation in the liquid. Everitt et al. [16] utilise a concentration potential $\phi(x, t)$, where $\partial\phi/\partial x = c - c_0$ for initial gas concentration c_0, in order to overcome numerical issues resulting from the steep concentration gradient at early time. The diffusion of this concentration potential is given as [16]

$$\frac{\partial \phi}{\partial t} = 9D(x+u)^{\frac{4}{3}}\frac{\partial^2\phi}{\partial x^2}, \tag{2.17}$$

where D is the diffusion coefficient. Applying the principle of mass conservation and the ideal gas law [2], then Eq. (2.17) can be manipulated to yield [16]

$$p_g u = p_{g_0}u(0) + R_g T\phi(0,t), \tag{2.18}$$

where p_{g_0} is the initial bubble gas pressure, $p_g = p_g(t)$ is the bubble gas pressure at subsequent $t > 0$, R_g is the universal gas constant and T is the temperature. The system is now fully described by (2.13), (2.14), (2.16), (2.17) and (2.18). Note that the system model presented here reduces to the model presented in [16] by setting $\rho = 0$ and $p_u = 0$ in the momentum Eq. (2.13).

The governing equations and boundary conditions are non-dimensionalised by substituting for the following non-dimensional variables: $\hat{t} = t/\tau$, $\hat{u} = u/u(0)$, $\hat{x} = x/u(0)$, $\hat{X} = X/u(0)$, $\hat{\phi} = \phi R_g T/(p_{g0}u(0))$, $P_g = (p_g - p_a)/(p_{g_0} - p_a)$, and $P_u = p_u/(p_{g_0} - p_a)$. For convenience, the following non-dimensional grouped parameters are then introduced [16]: the time-scale ratio, $N = 9D\tau/u(0)^{2/3}$, giving the ratio of the polymer relaxation time to gas diffusion time; the Deborah number, $De = (p_{g_0} - p_a)\tau/\mu$, giving the ratio of bubble growth in the solvent to the relaxation rate of the polymer; the viscosity ratio, $\gamma = G\tau/\mu$, giving the ratio of polymer contributions to the steady shear viscosity to those contributions from the solvent; the capillary number, $\Gamma = \mu u(0)^{1/3}/2S\tau$, giving the ratio of viscous force to surface tension, and the Reynolds number, $\mathcal{R} = \rho u(0)^{2/3}/3\mu\tau$, giving the ratio of inertial forces to viscous forces. This definition of the Reynolds number utilises the initial bubble radius, $u(0)^{1/3}$, as the characteristic length-scale and the polymer relaxation time, τ, as the time-scale; this gives the characteristic fluid velocity, $u(0)^{1/3}/\tau$, as the relaxation velocity for the initial bubble. For notational simplicity the $\hat{}$ symbol on the non-dimensionalised variables is now dropped. The resulting non-dimensionalised system is then given as

$$\frac{4}{3}\dot{u}\left(\frac{1}{u} - \frac{1}{(X+u)}\right) + \mathcal{R}\left[\ddot{u}\left(\frac{1}{u^{\frac{1}{3}}} - \frac{1}{(X+u)^{\frac{1}{3}}}\right) - \frac{\dot{u}^2}{6}\left(\frac{1}{u^{\frac{4}{3}}} - \frac{1}{(X+u)^{\frac{4}{3}}}\right)\right] = De(P_g - P_u) + \frac{2}{3}\gamma\int_0^X \frac{(A_{rr}-A_{\theta\theta})}{(x+u)}dx - \frac{1}{\Gamma u^{\frac{1}{3}}}, \tag{2.19}$$

$$\frac{\partial A_{rr}}{\partial t} = -\frac{4\dot{u}}{3(x+u)}A_{rr} - (A_{rr}-1), \tag{2.20}$$

$$\frac{\partial A_{\theta\theta}}{\partial t} = \frac{2\dot{u}}{3(x+u)}A_{\theta\theta} - (A_{\theta\theta}-1), \tag{2.21}$$

$$\frac{(p_a + (p_{g_0} - p_a)P_g)}{p_{g_0}}u = (1+\phi(0,t)), \tag{2.22}$$

$$\frac{\partial \phi}{\partial t} = N(x+u)^{\frac{4}{3}}\frac{\partial^2\phi}{\partial x^2}, \tag{2.23}$$

where the boundary conditions on $\phi(x, t)$ are,

$$\left.\frac{\partial\phi}{\partial x}\right|_{x=0} = \Phi\frac{(p_{g0}-p_a)}{p_{g_0}}(P_g - 1),$$

$$\left.\frac{\partial^2\phi}{\partial x^2}\right|_{x=X} = 0,$$

where $\Phi = R_g TH$ and H is the Henry's law constant. The non-dimensional initial conditions are,

$$u(0) = 1, \quad P_g(0) = 1, \quad A_{rr}(x,0) = 1, \quad A_{\theta\theta}(x,0) = 1, \quad \text{and} \quad \phi(0,0) = 0.$$

Everitt et al. [16] state that diffusion is approximately instantaneous in the limit $N \gg DeX^{2/3}$. By definition of the non-dimensional parameters this condition is equivalent to the requirement that $9D/u(0)^{2/3} \gg X^{2/3}(p_{g_0} - p_a)/\mu$, which states that the rate of gas diffusion is much larger than a grouped term dependent on the rate of bubble growth in the solvent and the fluid volume. The rate of gas diffusion is large in cases where the diffusivity is substantially larger than the surface area of the bubble; consider a fixed flow-rate of gas molecules into the bubble, then reducing the surface area will increase the speed at which individual particles flow into the bubble and so increase the rate of gas diffusion. A smaller bubble growth rate occurs when the pressure difference between the gas inside the bubble and the surrounding fluid is smaller, and the viscosity of the surrounding fluid is larger. A smaller pressure difference will reduce the outward tendency of the bubble to expand, and a larger viscosity will increase the inward tendency of the fluid to resist the bubble expansion. As the bubble growth rate decreases, the change in bubble volume decreases, and so for a fixed diffusivity the concentration of gas inside the bubble will increase more rapidly. A smaller fluid volume indicates that the gas in the fluid is in closer proximity to the bubble, and so for a fixed flow velocity the gas will diffuse into the bubble faster. Applying the instantaneous diffusion assumption here enables the analysis to be simplified by decoupling the equation in $\phi(x, t)$. Consideration of mass conservation of the gas then leads to

$$P_g = \frac{A + Bu + \Phi X}{u + \Phi X}, \tag{2.24}$$

where $A = p_{g_0}/(p_{g_0} - p_a)$ and $B = -p_a/(p_{g_0} - p_a)$. Note that setting $P_g = 0$ in Eq. (2.24) recovers precisely the expression given in [16] for the equilibrium bubble size, u_∞. In the following section multiscale analysis and asymptotic expansions are employed to investigate the effect of the inertia related term $\mathcal{R}$ on the early time and large time solutions. Asymptotic expansions are used to derive an inner solution (small time) for times $t = O(\eta)$ and then to construct an outer solution (large time) where η is a factor used to stretch the inner time variable.

3. Asymptotic analysis: inner solution

There is a brief time, which is assumed to be $O(\eta)$, in which the bubble volume rapidly increases from its initial value to a value that is commensurate with the outer solution derived in Section 4. In this phase of the bubble growth the inertia term dominates. To allow this behaviour to be studied, time is stretched by introducing the inner variable,

$$\vartheta = \frac{t}{\eta},$$

where η is a scaling constant such that $0 < \eta \ll 1$. For clarity the following notation is introduced for the inner solution $U(\vartheta, \eta) = u(t, \eta)$, $AR(x, \vartheta, \eta) = A_{rr}(x, t, \eta)$, $AQ(x, \vartheta, \eta) = A_{\theta\theta}(x, t, \eta)$, $P(\vartheta, \eta) = P_g(t, \eta)$ and $\phi(x, \vartheta, \eta) = \phi(x, t, \eta)$. As before instantaneous diffusion is assumed and expansions of the form,

$$U(\vartheta, \eta) = U_0(\vartheta) + \eta U_1(\vartheta) + O(\eta^2), \tag{3.1}$$

$$AR(x, \vartheta, \eta) = AR_0(x, \vartheta) + \eta AR_1(x, \vartheta) + O(\eta^2), \tag{3.2}$$

$$AQ(x, \vartheta, \eta) = AQ_0(x, \vartheta) + \eta AQ_1(x, \vartheta) + O(\eta^2), \tag{3.3}$$

and

$$P(\vartheta, \eta) = P_0(\vartheta) + \eta P_1(\vartheta) + O(\eta^2), \tag{3.4}$$

are substituted. By making the appropriate Taylor series expansions the momentum Eq. (3.1) is

$$\begin{aligned}
&\mathcal{R}\left(\ddot{U}_0\left(\frac{1}{U_0^{\frac{1}{3}}} - \frac{1}{(X+U_0)^{\frac{1}{3}}}\right) - \frac{\dot{U}_0^2}{6}\left(\frac{1}{U_0^{\frac{4}{3}}} - \frac{1}{(X+U_0)^{\frac{4}{3}}}\right)\right)\\
&+\eta\left[\frac{4}{3}\dot{U}_0\left(\frac{1}{U_0} - \frac{1}{X+U_0}\right) + \mathcal{R}\left(\ddot{U}_1\left(\frac{1}{U_0^{\frac{1}{3}}} - \frac{1}{(X+U_0)^{\frac{1}{3}}}\right)\right.\right.\\
&-\frac{\ddot{U}_0 U_1}{3}\left(\frac{1}{U_0^{\frac{4}{3}}} - \frac{1}{(X+U_0)^{\frac{4}{3}}}\right) + \frac{2\dot{U}_0^2 U_1}{9}\left(\frac{1}{U_0^{\frac{7}{3}}} - \frac{1}{(X+U_0)^{\frac{7}{3}}}\right)\\
&\left.\left.-\frac{\dot{U}_0\dot{U}_1}{3}\left(\frac{1}{U_0^{\frac{4}{3}}} - \frac{1}{(X+U_0)^{\frac{4}{3}}}\right)\right)\right] + O(\eta^2) = 0.
\end{aligned} \tag{3.5}$$

Note that following these expansions, the ultrasound pressure amplitude term, P_u, appearing in Eq. (2.19) is found to be of $O(\eta^2)$ and is therefore omitted from Eq. (3.5). This indicates that the ultrasound pressure field has little effect on the early stages of bubble growth. The rate equations for AR and AQ can be treated in a similar manner; the non-dimensionalised rate equation in $AR(x, \vartheta)$ is then

$$\begin{aligned}
\frac{\partial AR_0}{\partial \vartheta} + \eta\frac{\partial AR_1}{\partial \vartheta} = &\left(-\frac{4\dot{U}_0 AR_0}{3(x+U_0)}\right) + \eta\left[-\frac{4}{3(x+U_0)}\left(\dot{U}_0 AR_1\right.\right.\\
&\left.\left.-\frac{\dot{U}_0 AR_0 U_1}{(x+U_0)} + \dot{U}_1 AR_0\right) - (AR_0 - 1)\right] + O(\eta^2),
\end{aligned} \tag{3.6}$$

and

$$\begin{aligned}
\frac{\partial AQ_0}{\partial \vartheta} + \eta\frac{\partial AQ_1}{\partial \vartheta} = &\left(\frac{2\dot{U}_0 AQ_0}{3(x+U_0)}\right) + \eta\left[\frac{2}{3(x+U_0)}\left(\dot{U}_0 AQ_1\right.\right.\\
&\left.\left.-\frac{\dot{U}_0 AQ_0 U_1}{(x+U_0)} + \dot{U}_1 AQ_0\right) - (AQ_0 - 1)\right] + O(\eta^2).
\end{aligned} \tag{3.7}$$

The pressure and diffusion equations are given by

$$\begin{aligned}
P_0 + \eta P_1 = &\frac{A + BU_0 + \Phi X}{U_0 + \Phi X} + \eta\left(\frac{BU_1}{U_0 + \Phi X} - \frac{(A + BU_0 + \Phi X)U_1}{(U_0 + \Phi X)^2}\right)\\
&+O(\eta^2)
\end{aligned} \tag{3.8}$$

and

$$\phi_0 + \eta\phi_1 = \Phi\frac{p_{g_0} - p_a}{p_{g_0}}(P_0 - 1)X + \eta\left(\Phi\frac{p_{g_0} - p_a}{p_{g_0}}P_1 X\right) + O(\eta^2). \tag{3.9}$$

3.1. Leading order solution

Assuming that $\mathcal{R} \gg \eta$ then the leading order system is

$$\ddot{U}_0 U_0 (X+U_0)\left((X+U_0)^{\frac{1}{3}} - U_0^{\frac{1}{3}}\right) - \frac{\dot{U}_0^2}{6}\left((X+U_0)^{\frac{4}{3}} - U_0^{\frac{4}{3}}\right) = 0, \tag{3.10}$$

$$\frac{\partial AR_0}{\partial \vartheta} = -\frac{4}{3}\frac{\dot{U}_0}{(x+U_0)}AR_0, \tag{3.11}$$

$$\frac{\partial AQ_0}{\partial \vartheta} = \frac{2}{3}\frac{\dot{U}_0}{(x+U_0)}AQ_0, \tag{3.12}$$

$$P_0 = \frac{A + BU_0 + \Phi X}{U_0 + \Phi X}, \tag{3.13}$$

and

$$\phi_0 = \Phi\frac{p_{g_0} - p_a}{p_{g_0}}P_0 X, \tag{3.14}$$

with initial conditions $U_0(0) = 1$, $AR_0(x, 0) = 1$, $AQ_0(x, 0) = 1$, $\phi_0(0) = 0$, $P_0(0) = 1$, and $\dot{U}_0(0) = c_v$, where $c_v > 0$ is the initial rate of change of the volume. Since the early time evolution of the bubble is of interest, it is assumed that $U_0 \ll X$ and Eq. (3.10) reduces to

$$\ddot{U}_0 U_0 - \frac{\dot{U}_0^2}{6} = 0. \tag{3.15}$$

This can be transformed using $U_0(\vartheta) = e^{az(\vartheta)}$ to give

$$\ddot{z} + \frac{5a}{6}\dot{z}^2 = 0.$$

Choosing $a = 6/5$ results in the second order, non-linear, ODE in z,

$$\ddot{z} + \dot{z}^2 = 0.$$

Making another substitution, $y = \dot{z}$, reduces this to a first order equation which can be integrated. Applying the initial conditions $U_0(0) = 1$ and $\dot{U}_0(0) = c_v$ (where $c_v > 0$) leads to

$$U_0 = \left(1 + \frac{5c_v}{6}\vartheta\right)^{\frac{6}{5}}. \tag{3.16}$$

Turning to the orientation tensor, the zero order rate Eqs. (3.11) and (3.12) can each be solved by separating variables. Looking first at AR_0, application of the initial conditions $AR_0(x, 0) = 1$

and $U_0(0) = 1$ gives

$$AR_0(x,\vartheta) = \left(\frac{x+1}{x+(1+5c_v\vartheta/6)^{\frac{6}{5}}}\right)^{\frac{4}{3}}. \tag{3.17}$$

In the same way AQ_0 is

$$AQ_0(x,\vartheta) = \left(\frac{x+(1+5c_v\vartheta/6)^{\frac{6}{5}}}{x+1}\right)^{\frac{2}{3}}. \tag{3.18}$$

Eqs. (3.16) and (3.13) then give the leading order pressure solution, P_0, as

$$P_0 = \frac{A+B(1+5c_v\vartheta/6)^{\frac{6}{5}}+\Phi X}{(1+5c_v\vartheta/6)^{\frac{6}{5}}+\Phi X}, \tag{3.19}$$

and the diffusion equation to leading order, ϕ_0, follows directly from Eq. (3.14).

3.2. First order solution

Having constructed the leading order solution, derivations are sought for the first order term U_1. Taking terms of order η in (3.5), (3.6), (3.7), (3.8) and (3.9) results in the first order system,

$$\begin{aligned}&\ddot{U}_1\left(\frac{1}{U_0^{\frac{1}{3}}}-\frac{1}{(X+U_0)^{\frac{1}{3}}}\right)-\dot{U}_1\frac{\dot{U}_0}{3}\left(\frac{1}{U_0^{\frac{4}{3}}}-\frac{1}{(X+U_0)^{\frac{4}{3}}}\right)\\&+U_1\left(\frac{2\dot{U}_0^2}{9}\left(\frac{1}{U_0^{\frac{7}{3}}}-\frac{1}{(X+U_0)^{\frac{7}{3}}}\right)-\frac{\ddot{U}_0}{3}\left(\frac{1}{U_0^{\frac{4}{3}}}-\frac{1}{(X+U_0)^{\frac{4}{3}}}\right)\right)\\&+\frac{4\dot{U}_0}{3\mathcal{R}}\left(\frac{1}{U_0}-\frac{1}{(X+U_0)}\right)=0,\end{aligned} \tag{3.20}$$

$$\begin{aligned}\frac{\partial AR_1}{\partial\vartheta} &= -\frac{4}{3(x+U_0)}\left(\dot{U}_1AR_0-U_1\frac{\dot{U}_0AR_0}{(x+U_0)}+\dot{U}_0AR_1\right)\\&\quad-(AR_0-1),\end{aligned} \tag{3.21}$$

$$\begin{aligned}\frac{\partial AQ_1}{\partial\vartheta} &= \frac{2}{3(x+U_0)}\left(\dot{U}_1AQ_0-U_1\frac{\dot{U}_0AQ_0}{(x+U_0)}+\dot{U}_0AQ_1\right)\\&\quad-(AQ_0-1),\end{aligned} \tag{3.22}$$

$$P_1 = \frac{U_1}{U_0+\Phi X}\left(B-\frac{A+BU_0+\Phi X}{U_0+\Phi X}\right), \tag{3.23}$$

and

$$\phi_1 = \Phi\frac{p_{g_0}-p_a}{p_{g_0}}P_1X. \tag{3.24}$$

Eq. (3.20) can be expressed as

$$\ddot{U}_1+\frac{\mathbb{N}_2}{\mathbb{N}_1}\dot{U}_1+\frac{\mathbb{N}_3}{\mathbb{N}_1}U_1+\frac{\mathbb{N}_4}{\mathbb{N}_1}=0, \tag{3.25}$$

where,

$$\mathbb{N}_1 = \frac{1}{U_0^{\frac{1}{3}}}-\frac{1}{(X+U_0)^{\frac{1}{3}}},$$

$$\mathbb{N}_2 = -\frac{\dot{U}_0}{3}\left(\frac{1}{U_0^{\frac{4}{3}}}-\frac{1}{(X+U_0)^{\frac{4}{3}}}\right),$$

$$\mathbb{N}_3 = \frac{2\dot{U}_0^2}{9}\left(\frac{1}{U_0^{\frac{7}{3}}}-\frac{1}{(X+U_0)^{\frac{7}{3}}}\right)-\frac{\ddot{U}_0}{3}\left(\frac{1}{U_0^{\frac{4}{3}}}-\frac{1}{(X+U_0)^{\frac{4}{3}}}\right),$$

and

$$\mathbb{N}_4 = \frac{4\dot{U}_0}{3\mathcal{R}}\left(\frac{1}{U_0}-\frac{1}{X+U_0}\right).$$

The expressions for $\mathbb{N}_i, i=1,\cdots,4$ can be expanded in $1/X$ giving the leading order terms,

$$\frac{\mathbb{N}_2}{\mathbb{N}_1} = -\frac{\dot{U}_0}{3U_0} = -\frac{2c_v}{(6+5c_v\vartheta)},$$

$$\frac{\mathbb{N}_3}{\mathbb{N}_1} = \frac{2\dot{U}_0^2}{9U_0^2}-\frac{\ddot{U}_0}{3U_0} = \frac{6c_v^2}{(6+5c_v\vartheta)^2},$$

and

$$\frac{\mathbb{N}_4}{\mathbb{N}_1} = \frac{4\dot{U}_0}{3\mathcal{R}U_0^{\frac{2}{3}}} = \frac{4c_v6^{\frac{3}{5}}}{3\mathcal{R}(6+5c_v\vartheta)^{\frac{3}{5}}}.$$

Substituting these coefficients into Eq. (3.25), transforming to the variable $z=(6+5c_v\vartheta)$ and multiplying by z^2 yields

$$z^2\ddot{U}_1-\frac{2}{5}z\dot{U}_1+\frac{6}{25}U_1 = -\frac{4z^{\frac{7}{5}}6^{\frac{3}{5}}}{75\mathcal{R}c_v}. \tag{3.26}$$

This is essentially the Euler differential equation [31], which solves to give the general solution as

$$U_1(z) = E_1z^{\frac{6}{5}}+E_2z^{\frac{1}{5}}-\frac{2(6^{\frac{3}{5}})}{9\mathcal{R}c_v}z^{\frac{7}{5}},$$

for constants E_1 and E_2. The initial conditions for the first order term $U_1(\vartheta)$ are $U_1(0)=\dot{U}_1(0)=0$ and in the transformed system $(U_1(z))$ these become $U_1(6)=\dot{U}_1(6)=0$, giving the particular solution

$$U_1(z) = \frac{2}{\mathcal{R}c_v}\left(\frac{4}{5(6^{\frac{1}{5}})}\left(z^{\frac{6}{5}}-z^{\frac{1}{5}}\right)-\frac{6^{\frac{3}{5}}}{9}z^{\frac{7}{5}}\right). \tag{3.27}$$

Rewriting in the original inner variable ϑ, and combining it with the leading order solution gives

$$\begin{aligned}U(\vartheta) &= \frac{2\eta}{\mathcal{R}c_v}\left(\frac{4}{5(6^{\frac{1}{5}})}\left((6+5c_v\vartheta)^{\frac{6}{5}}-(6+5c_v\vartheta)^{\frac{1}{5}}\right)\right.\\&\quad\left.-\frac{6^{\frac{3}{5}}}{9}(6+5c_v\vartheta)^{\frac{7}{5}}\right)+\left(1+\frac{5c_v}{6}\vartheta\right)^{\frac{6}{5}}.\end{aligned} \tag{3.28}$$

The effect of inertia can be examined by considering Eq. (3.5) for $\mathcal{R}=0$:

$$\frac{4}{3}\dot{U}\left(\frac{1}{U}-\frac{1}{X+U}\right)=0. \tag{3.29}$$

This has solution $U=c_v\vartheta+1$ where the initial conditions are given by $\dot{U}(0)=c_v$ and $U(0)=1$. Fig. 1 shows the effects of inertia on the bubble volume, U, in terms of the leading- and first-order solutions, and for comparison includes the system with no inertia, as given by Eq. (3.29). Note that the system with no inertia is essentially the system considered in [16], as the effects of the acoustic amplitude are also negligible in this early time analysis. It is also worth noting that the system considered in [45] incorporates the effects of inertia, although no results on these effects were presented. The timescale shown in Fig. 1 represents a range of 0–0.1 s, and the non-dimensional bubble volume is scaled with respect to the initial bubble volume (equal to 10^{-18} m^3). This Figure shows that as inertia increases (through increasing $\mathcal{R}$), the bubble volume, U, increases more rapidly and converges to the leading order solution $U_0=(1+5c_v\vartheta/6)^{6/5}$. For lower inertia ($\mathcal{R}=0.05$), the bubble volume increases approximately 65-fold over this early

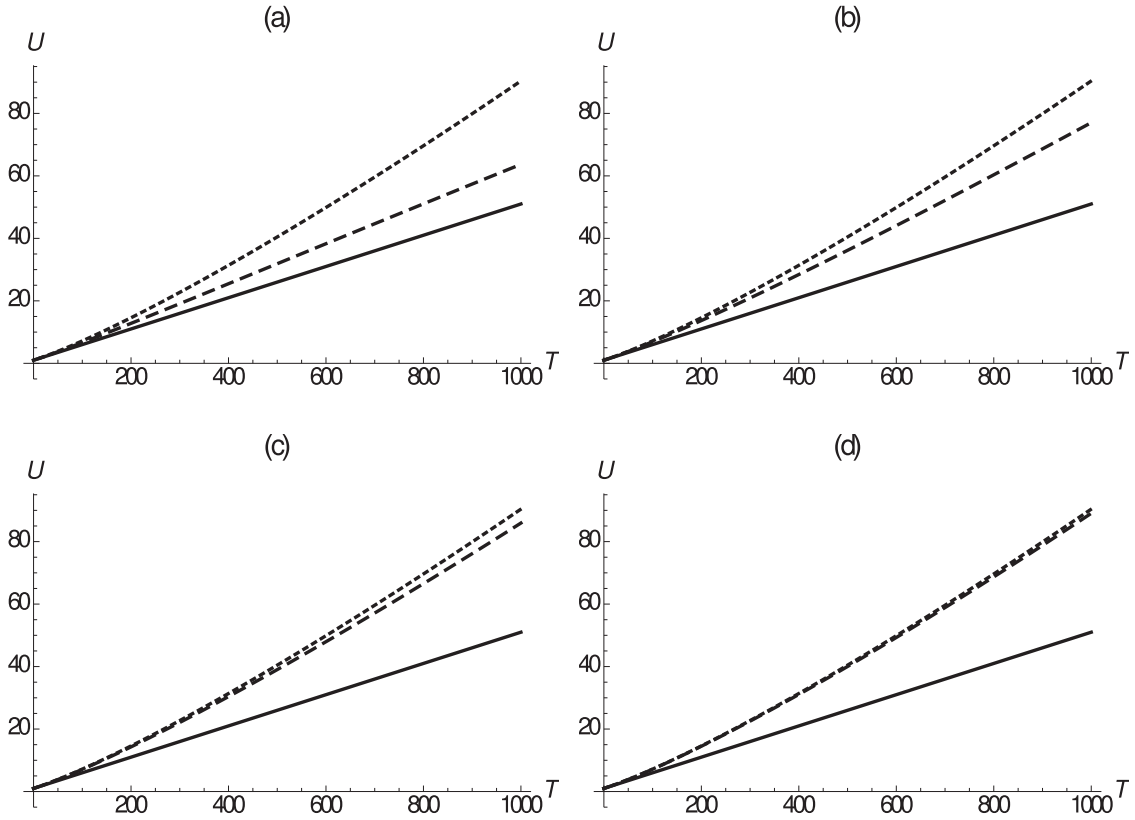

Fig. 1. Plots illustrating the following analytic solutions: the leading order solution given by Eq. (3.16) (dotted curve), the first order solution (dashed curve) given by Eq. (3.28) and the leading order solution in the case of negligible inertia, Eq. (3.29) (solid curve). In all cases $\eta = 10^{-4}$, $c_v = 0.05$ and $\mathcal{R} \gg \eta$. The parameter $\mathcal{R}$ is given by (a) $\mathcal{R} = 0.05$, (b) $\mathcal{R} = 0.1$, (c) $\mathcal{R} = 0.3$ and (d) $\mathcal{R} = 1.0$. These figures demonstrate that as $\mathcal{R}$ increases within this regime, the bubble volume increases more rapidly and converges to the leading order solution.

time period, whereas for higher inertia ($\mathcal{R} = 1.0$) the bubble volume increases approximately 90-fold over the same period.

Equipped with solutions (3.16) and (3.27), the first order pressure and diffusion equations (Eqs. (3.23) and (3.24), respectively) are now fully defined, and the first order rate equations for the orientation tensor (Eqs. (3.21) and (3.22)) can now be solved using the integrating factor method. Using Eqs. (3.16), (3.17), (3.27) and applying the initial condition $AR_1(x, 0) = 0$, the solution of Eq. (3.21) is found to be

$$AR_1(x, \vartheta) = (x + U_0)^{-\frac{4}{3}} \left(\widehat{AR}_1(x, \vartheta) - \widehat{AR}_1(x, 0) \right), \tag{3.30}$$

where

$$\widehat{AR}_1(x, \vartheta) = \frac{8(1+x)^{\frac{4}{3}}}{3\mathcal{R}c_v} \left(\frac{4}{U_0 + x} \left(U_0^{\frac{1}{6}} \left(U_0 + \frac{1}{5} \right) + \frac{6x}{5} \right) \right)$$
$$+ \frac{U_0^{\frac{5}{6}}}{455c_v} \left(-546(1+x)^{\frac{4}{3}} + 30(x + U_0)^{\frac{1}{3}} (15x + 7U_0) \right)$$
$$+ \frac{96x^{\frac{4}{3}} U_0^{\frac{5}{6}}}{455c_v} {}_2F_1 \left(\frac{2}{3}, \frac{5}{6}, \frac{11}{6}, -\frac{U_0}{x} \right)$$

and ${}_2F_1(a, b, c, z)$ denotes the ordinary (Gaussian) hypergeometric function [1]. Applying Eqs. (3.16), (3.18), (3.27) and the initial condition $AQ_1(x, 0) = 0$ in a similar fashion, solving Eq. (3.22) leads to

$$AQ_1(x, \vartheta) = (x + U_0)^{\frac{2}{3}} \left(\widehat{AQ}_1(x, \vartheta) - \widehat{AQ}_1(x, 0) \right), \tag{3.31}$$

where

$$\widehat{AQ}_1(x, \vartheta) = \frac{6U_0^{\frac{5}{6}}}{5c_v x^{\frac{2}{3}}} {}_2F_1 \left(\frac{2}{3}, \frac{5}{6}, \frac{11}{6}, -\frac{U_0}{x} \right)$$
$$- \frac{4}{3\mathcal{R}c_v (x+1)^{\frac{2}{3}}} \left[4U_0^{\frac{1}{6}} + \frac{9\mathcal{R}U_0^{\frac{5}{6}}}{10} \right.$$
$$\left. + \frac{12}{U_0 + x} \left(\frac{2x}{5} + \left(\frac{1}{15} - \frac{x}{3} \right) U_0^{\frac{1}{6}} \right) \right].$$

Solutions to first order can now be produced for the pressure and diffusion equations, and for the rate equations for the orientation tensor. Fig. 2 displays the time-varying pressure as the effect of inertia on the system is increased by increasing the value of $\mathcal{R}$. The non-dimensional pressure is the pressure difference between the gas and surrounding fluid scaled with respect to the initial pressure difference (where an initial difference of 900 kNm^{-2} is used), and the timescale shown in each plot is the range 0–1 s. Fig. 2(a) and (b) show that for smaller values of $\mathcal{R}$, the pressure initially decreases, before steadily increasing with time. An overall increase in the pressure difference of 30% and 4% are shown for $\mathcal{R} = 0.05$ and $\mathcal{R} = 0.1$, respectively, over this timescale. For larger $\mathcal{R}$ values the behaviour is quite different, with the pressure converging to the leading order behaviour for large $\mathcal{R}$. This is demonstrated in Fig. 2(c) and (d) where the pressure steadily decreases as time increases. The result shown is a reduction in the pressure difference of 10% and 20% for $\mathcal{R} = 0.3$ and $\mathcal{R} = 1.0$, respectively. Further investigations reveal that by reducing the value of η (thereby reducing the contribution of the first order component, and reducing the timescale in real terms), the pressure behaviour for each value of $\mathcal{R}$ is similar to that shown in Fig. 2(c) and (d). Note that the diffusion, which is simply a linear scaling of the pressure, exhibits a similar behaviour.

In Fig. 3, the behaviour surface of the non-dimensional radial stress, AR, is shown to first order for varying values of $\mathcal{R}$. The

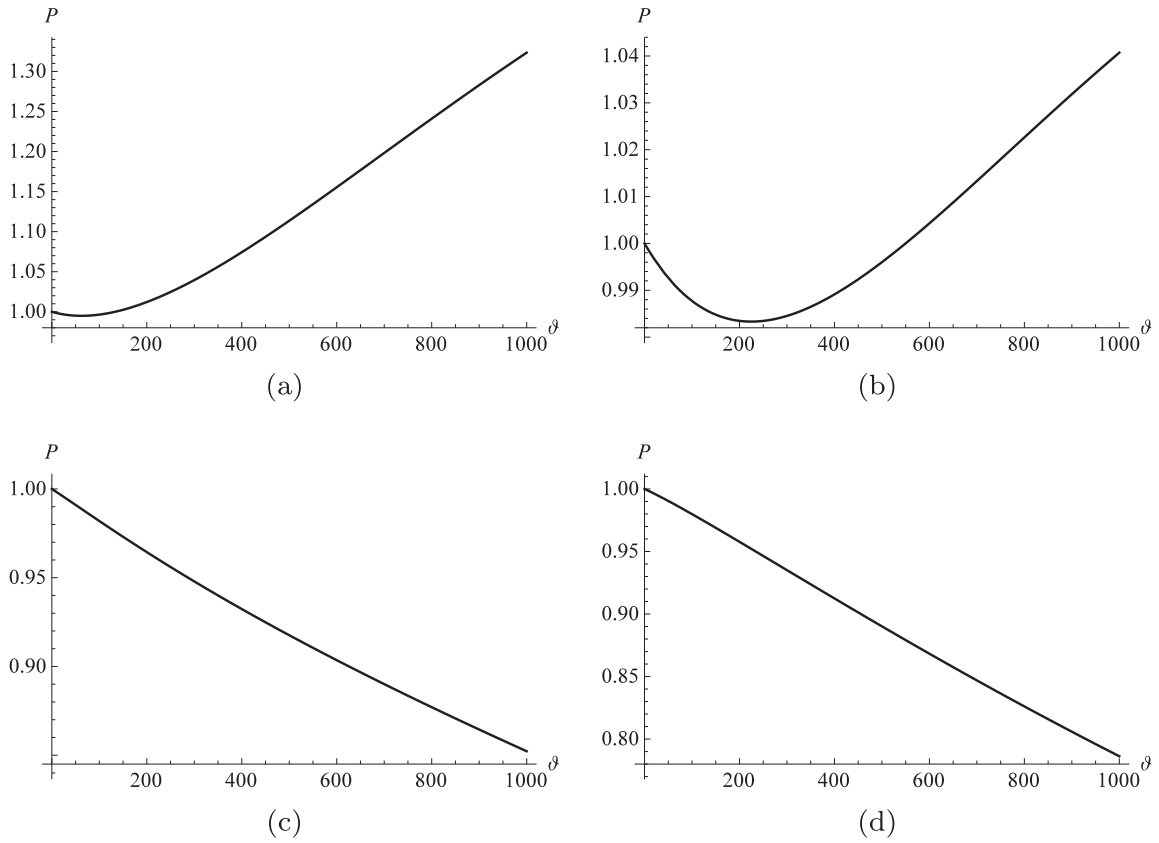

Fig. 2. Plots illustrating the non-dimensionalised pressure as given by Eqs. (3.4), (3.19) and (3.23). In all cases $\eta = 10^{-3}$, $c_v = 0.05$ and $\mathcal{R} \gg \eta$. The parameter $\mathcal{R}$ is given by (a) $\mathcal{R} = 0.05$, (b) $\mathcal{R} = 0.1$, (c) $\mathcal{R} = 0.3$ and (d) $\mathcal{R} = 1.0$. The remaining parameter values are as follows: $p_a = 10^5$, $p_{g0} = 10p_a$, Φ=0.32 and Γ=1000.

non-dimensional spatial variable, x, is scaled with respect to the initial bubble volume of 10^{-18} m^3, and is varied here up to ten-fold the initial bubble volume. In real terms the timescale used represents 0–1 s, and recall that the non-dimensionalised radial stress is initially equal to one throughout the fluid. The overall behaviour shown for each value of $\mathcal{R}$ is seen to be similar in each case. With respect to the non-dimensional time (ϑ), for small x the radial stress initially decreases sharply before increasing at a relatively steady rate. The rate of this increase reduces as x increases, and for larger x this increase is relatively minimal. The radial stress is shown to be less sensitive with respect to the distance from the bubble surface, x, however, there is a gradual increase in AR as x increases, which is most evident around the time at which AR first begins to increase. Increasing the inertia through increasing $\mathcal{R}$ is shown to have little impact for small x (that is, close to the bubble surface); however, for larger x, increasing inertia is shown to increase the severity of the initial decrease in AR (that is, for small ϑ). With $\mathcal{R} = 0.05$, the overall reduction in radial stress over the early time period is approximately 55% close to the bubble surface, and the reduction is approximately 40% far from the bubble surface. In comparison, with $\mathcal{R} = 1.0$, the overall reduction in radial stress over the early time period is approximately 55% close to the bubble surface, and approximately 60% reduction far from the bubble surface. Increased inertia therefore results in reduced radial stress at the steady-state of the system (for larger x and larger ϑ).

The non-dimensional circumferential (hoop) stress, AQ, is examined to first order in Fig. 4 for varying values of $\mathcal{R}$. As in Fig. 3, the timescale represents a range of 0–1 s in real terms, the non-dimensional spatial variable is varied from the initial bubble volume (equivalent to 10^{-18} m^3) up to a ten-fold increase of this volume, and the non-dimensional stress is initially equal to one throughout the fluid. Measured in a compression frame of reference, negative values indicate stretching in this case. The most interesting hoop stress behaviour is found to occur close to the bubble surface, where the effect of increasing inertia is shown to increase the extent of an initial phase of increasing compression (portrayed in Fig. 4 as a surface increasing above one), and subsequently reduce the extent of a second phase of increasing stretching (portrayed in Fig. 4 as a decreasing negative surface). Fig. 4(a) demonstrates that for comparatively small inertia ($\mathcal{R} = 0.05$), the hoop stress is largest close to the bubble surface and increases in magnitude with time; that is, AQ is most negative for smaller x and larger ϑ, and is close to zero outside this region. At the bubble surface the hoop stress shows an almost imperceptible increase for early time, followed by a steep decrease. This can be interpreted as a negligible increase in the magnitude of the circumferential compression stress, followed by an increase in the circumferential stretching stress to a value that is approximately 30-fold the initial compression stress. Fig. 4(b) demonstrates that as inertia increases the largest magnitude of the hoop stress decreases, indicating reduced stress due to expansion. An additional observation is that, in comparison with Fig. 4(a), close to the bubble surface the initial compression phase of the hoop stress is shown to be slightly increased, and the subsequent stretching phase of the hoop stress is not so extreme. Each of these effects becomes increasingly prominent as the effect of inertia is increased further in Fig. 4(c) and (d), with larger initial increases in the hoop stress close to the bubble surface, followed by smaller decreases as the bubble evolves. The result is that in Fig. 4(d) with $\mathcal{R} = 1.0$, the hoop stress at the bubble surface is shown to gradually increase then decrease, whilst remaining above one (the initial stress value) throughout. This behaviour can be interpreted as a steady increase in the circumferen-

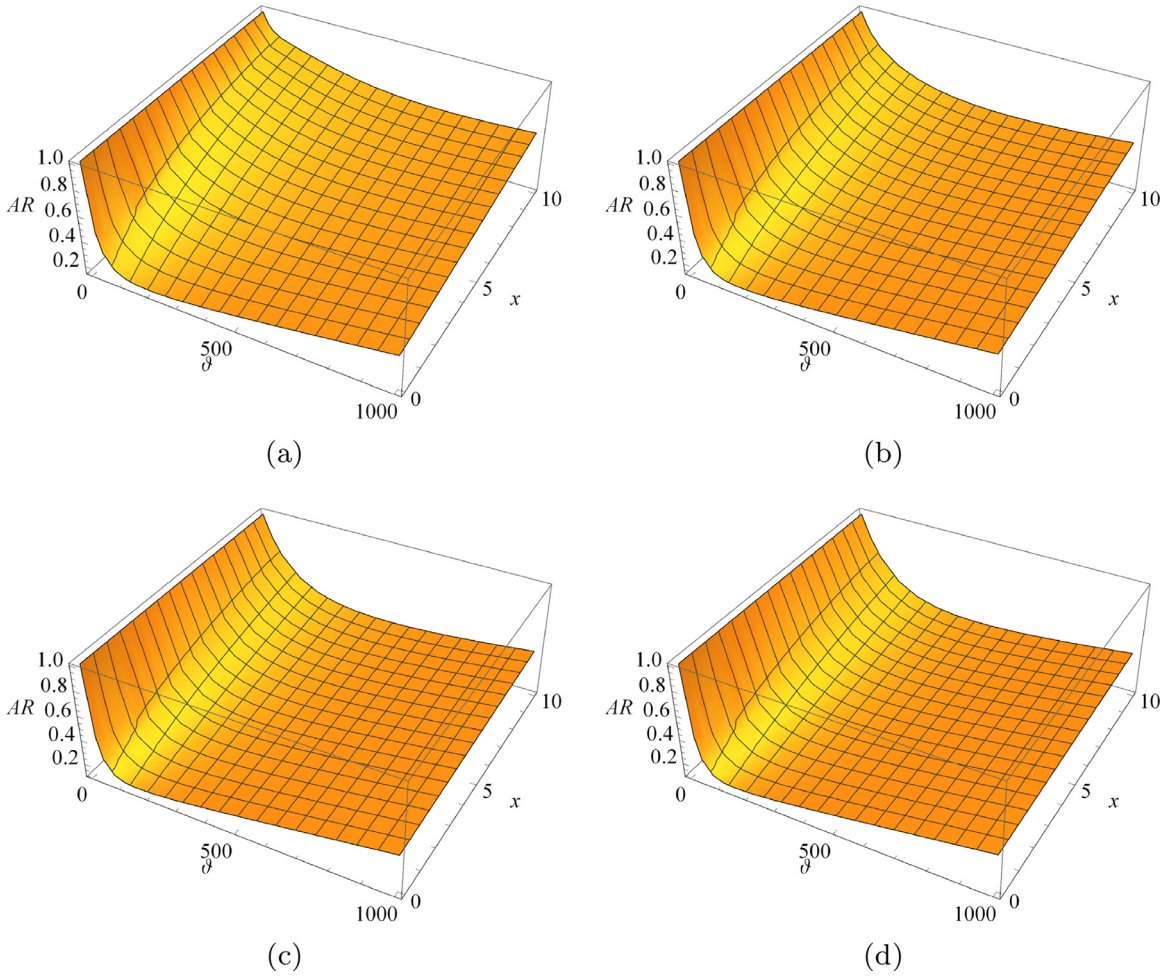

Fig. 3. Plots illustrating the non-dimensionalised radial stress as given by Eqs. (3.2), (3.17) and (3.30). In all cases $\eta = 10^{-3}$, $c_v = 0.05$ and $\mathcal{R} \gg \eta$. The parameter $\mathcal{R}$ is given by (a) $\mathcal{R} = 0.05$, (b) $\mathcal{R} = 0.1$, (c) $\mathcal{R} = 0.3$ and (d) $\mathcal{R} = 1.0$.

tial compression stress to a value approximately six-fold the initial stress value, followed by a gradual relaxation of this stress as it returns to approximately the initial value. In this case, no circumferential stretching stress is observed over this timescale, indicating that only compression is occurring here.

4. Asymptotic analysis: outer solution

For the outer solution expansions are made in the Reynolds number, $\mathcal{R}$, noting the scaling assumption made for the inner solution, namely, $\mathcal{R} \gg \eta$. An expansion in the outer temporal variable, t, is therefore sought in the form

$$u(t, \mathcal{R}) = u_0(t) + \mathcal{R}u_1(t) + O(\mathcal{R}^2), \tag{4.1}$$

$$A_{rr}(x, t, \mathcal{R}) = A_{rr_0}(x, t) + \mathcal{R}A_{rr_1}(x, t) + O(\mathcal{R}^2), \tag{4.2}$$

and

$$A_{\theta\theta}(x, t, \mathcal{R}) = A_{\theta\theta_0}(x, t) + \mathcal{R}A_{\theta\theta_1}(x, t) + O(\mathcal{R}^2). \tag{4.3}$$

Substituting Eq. (4.1) in Eq. (2.24) the expansion for P_g can be derived as follows

$$\begin{aligned} P_g &= \left(\frac{A + Bu_0 + \Phi X}{u_0 + \Phi X}\right) + \mathcal{R}\left(\frac{Bu_1}{u_0 + \Phi X} - \frac{u_1(A + Bu_0 + \Phi X)}{(u_0 + \Phi X)^2}\right) \\ &\quad + O(\mathcal{R}^2), \\ &= P_{g_0} + \mathcal{R}P_{g_1} + O(\mathcal{R}^2). \end{aligned}$$

Using these expressions to leading order in $\mathcal{R}$, the momentum Eq. (2.19) is

$$\begin{aligned} \frac{4}{3}\dot{u}_0\left(\frac{1}{u_0} - \frac{1}{X + u_0}\right) &= De(P_{g_0} - P_u) \\ &\quad + \frac{2}{3}\gamma\int_0^X \frac{(A_{rr} - A_{\theta\theta})_0}{x + u_0}dx - \frac{1}{\Gamma u_0^{\frac{1}{3}}}. \end{aligned} \tag{4.4}$$

In the same way, expanding Eqs. (2.20) and (2.21) using (4.2) and (4.3) gives to leading order in $\mathcal{R}$

$$\frac{\partial A_{rr_0}}{\partial t} = -\frac{4}{3}\frac{\dot{u}_0 A_{rr_0}}{(x + u_0)} - (A_{rr_0} - 1). \tag{4.5}$$

and

$$\frac{\partial A_{\theta\theta_0}}{\partial t} = \frac{2}{3}\frac{\dot{u}_0 A_{\theta\theta_0}}{(x + u_0)} - (A_{\theta\theta_0} - 1). \tag{4.6}$$

The initial conditions are $u_0(t^*) = u_0^*$, $P_{g_0}(t^*) = P_{g_0}^*$, $A_{rr_0}(x, t^*) = A_{rr_0}^*(x)$, $A_{\theta\theta_0}(x, t^*) = A_{\theta\theta_0}^*(x)$ and $\phi_0(t^*) = \phi_0^*$, where the starred constants are to be determined from the inner solution by matching these two asymptotic expansions.

Employing the integrating factor method in Eq. (4.5) leads to

$$\begin{aligned} A_{rr_0}(x, t) &= e^{-t}(x + u_0)^{-\frac{4}{3}}\int_{t^*}^t e^{\hat{t}}(x + u_0)^{\frac{4}{3}}d\hat{t} \\ &\quad + A_{rr_0}^*(x)e^{t^* - t}\left(\frac{x + u_0^*}{x + u_0}\right)^{\frac{4}{3}}. \end{aligned}$$

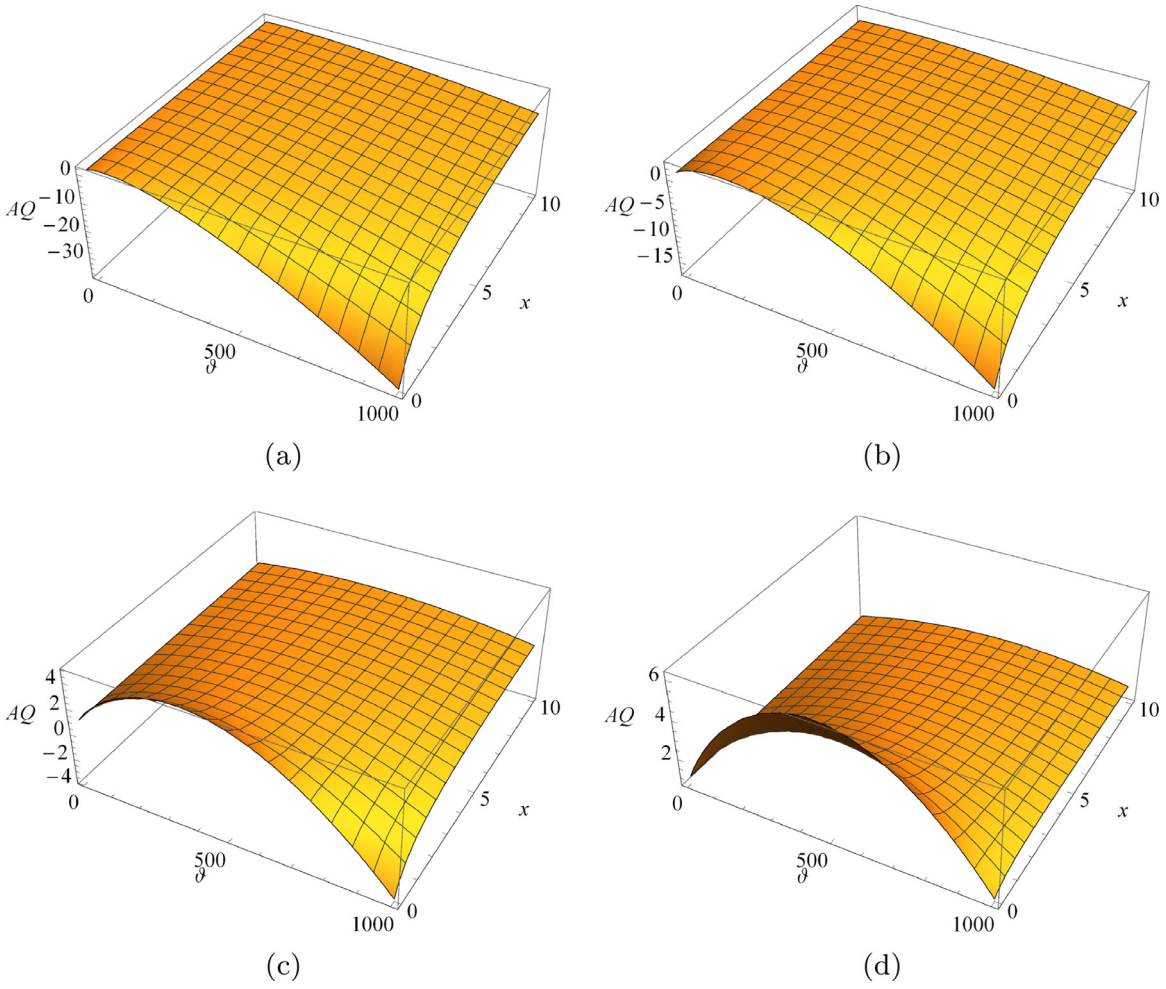

Fig. 4. Plots illustrating the non-dimensionalised circumferential stress as given by Eqs. (3.3), (3.18) and (3.31). In all cases $\eta = 10^{-3}$, $c_v = 0.05$ and $\mathcal{R} \gg \eta$. The parameter $\mathcal{R}$ is given by (a) $\mathcal{R} = 0.05$, (b) $\mathcal{R} = 0.1$, (c) $\mathcal{R} = 0.3$ and (d) $\mathcal{R} = 1.0$.

Similarly, Eq. (4.6) leads to

$$\begin{aligned}(A_{rr} - A_{\theta\theta})_0(x,t) = e^{-t}\Bigg[&(x+u_0)^{-\frac{4}{3}}\int_{t^*}^{t} e^{\hat{t}}(x+u_0)^{\frac{4}{3}}d\hat{t}\\ &-(x+u_0)^{\frac{2}{3}}\int_{t^*}^{t} e^{\hat{t}}(x+u_0)^{-\frac{2}{3}}d\hat{t}\\ &+e^{t^*}\left(A^*_{rr_0}(x)\left(\frac{x+u_0^*}{x+u_0}\right)^{\frac{4}{3}}\right.\\ &\left.-A^*_{\theta\theta_0}(x)\left(\frac{x+u_0}{x+u_0^*}\right)^{\frac{2}{3}}\right)\Bigg].\end{aligned}$$

Hence,

$$\begin{aligned}I(u_0,x,t) &= \frac{(A_{rr} - A_{\theta\theta})_0(x,t)}{(x+u_0)},\\ &= I_1(u_0,x,t) - I_2(u_0,x,t) + I_3(u_0,x,t),\end{aligned} \tag{4.7}$$

$$\begin{aligned}&= f_1(u_0,x,t)\int_{t^*}^{t} k_1(u_0,x,\hat{t})d\hat{t}\\ &\quad -f_2(u_0,x,t)\int_{t^*}^{t} k_2(u_0,x,\hat{t})d\hat{t} + f_3(u_0,x,t),\end{aligned} \tag{4.8}$$

where,

$$f_1(u_0,x,t) = e^{-t}(x+u_0)^{-\frac{7}{3}},$$

$$f_2(u_0,x,t) = e^{-t}(x+u_0)^{-\frac{1}{3}},$$

$$\begin{aligned}f_3(u_0,x,t) = e^{t^*-t}\Big(&A^*_{rr_0}(x)(x+u_0^*)^{\frac{4}{3}}(x+u_0)^{-\frac{7}{3}}\\ &-A^*_{\theta\theta_0}(x)(x+u_0^*)^{-\frac{2}{3}}(x+u_0)^{-\frac{1}{3}}\Big),\end{aligned}$$

$$k_1(u_0,x,\hat{t}) = e^{\hat{t}}(x+u_0)^{\frac{4}{3}},$$

and

$$k_2(u_0,x,\hat{t}) = e^{\hat{t}}(x+u_0)^{-\frac{2}{3}}.$$

To leading order, the momentum Eq. (4.4) is of the form

$$\dot{u}_0 = g(u_0,t),$$

and an approximate solution can be found using the Picard iteration method [7]. The first Picard iterate, $u_0^{p1}(t)$, is derived analytically and a numerical algorithm is produced to test the accuracy of this first analytic iteration. The first iteration of the Picard method is given by,

$$u_0^{p1}(t) = u_0^* + \int_{t^*}^{t} g(u_0^*,t)dt, \tag{4.9}$$

where $u_0^* = u_0(t^*)$.

Plots of this leading order analytic Picard approximation are illustrated in Fig. 5 (a) and (b), for a range of values of P_u and De, respectively. The grouped parameter De is the ratio of the bubble growth rate to the relaxation rate of the polymer and is inversely proportional to the viscosity value μ. Fig. 5 (b) shows that

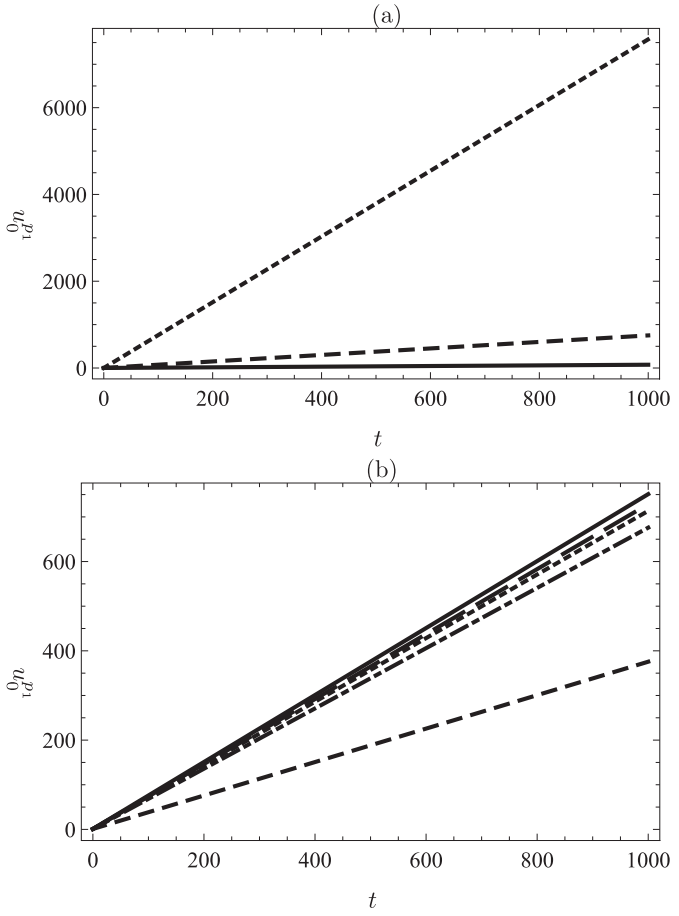

Fig. 5. Plots of the first Picard iterate solution, u_0^{p1} given by Eq. (4.9), for a range of values of (a) *De* (which is inversely proportional to viscosity) and (b) P_u, the non-dimensional value for the pressure amplitude of the irradiating acoustic standing wave. The initial conditions and parameters common to both plots are as follows: $t^* = 0$, $u^* = 1$, $X = 1000$, $p_a = 10^5$, $p_{g_0} = 10p_a$, $\Phi = 0.32$, $\Gamma = 1000$. In (a) $P_u = 0$ and the range of values for *De* are 0.1 (solid line), 1 (dashed line), 10 (dotted line), and in (b) the non-dimensional pressure amplitude values, P_u, are zero (solid line), 0.03 (long-dashed line), 0.05 (dotted line), 0.10 (dot-dashed line), 0.50 (short-dashed line), with *De* fixed at 1.

as viscosity decreases, for a constant initial gas pressure difference across the bubble wall, the initial bubble growth rate increases as expected. The next section will show, however, that although the numerical solution predicts the same qualitative increase, it asymptotes to a steady state value, whereas the Picard solution does not. This is not unexpected since only one iteration of the Picard scheme has been carried out to retrieve the leading order linear solution (4.9). This leading order solution is relatively accurate near to the inital bubble volume but as t increases it is less so, as illustrated in Fig. 7. The Picard method is a function-wise iteration and would require several more iterations to produce a reasonable approximation over a larger domain interval. Theoretically this is possible, but due to the complexity of the system and the integro-differential momentum equation this analytical path is not pursued further.

The relationship between the irradiating acoustic standing wave pressure amplitude, P_u, and the final bubble volume can be observed in Fig. 5(a) and implies that increasing this amplitude suppresses the speed of bubble volume growth at early time. Since this linear approximation does not asymptote as the numerical solution is expected to do, the effect of the pressure amplitude on the steady state bubble volume cannot be predicted. This effect is investigated in the following section, where a numerical analysis is performed for the outer solution in the case of instantaneous diffusion.

4.1. Numerical solution of the leading order momentum equation

The momentum Eq. (4.4) contains an integral in t given by Eq. (4.8) within an integral over x. For the temporal integrals within the integrand $I(u_0, x, t)$ a quadrature rule is used with weightings α_k, where $u_{0k} = u_0(\hat{t}_k)$, $\hat{t}_1 = t^*$, $\hat{t}_j = t_j$ and $t_j \in [t^*, t]$ to give,

$$I_1(u_{0j}, x, t_j) = e^{-t_j}(x + u_{0j})^{-\frac{7}{3}} \sum_{k=1}^{j} \alpha_k e^{\hat{t}_k}(x + u_{0k})^{\frac{4}{3}},$$

$$I_2(u_{0j}, x, t_j) = e^{-t_j}(x + u_{0j})^{-\frac{1}{3}} \sum_{k=1}^{j} \alpha_k e^{\hat{t}_k}(x + u_{0k})^{-\frac{2}{3}},$$

$$I_3(u_{0j}, x, t_j) = e^{t^*-t_j}\Big(A^*_{rr_0}(x)(x + u_{0j}^*)^{\frac{4}{3}}(x + u_0)^{-\frac{7}{3}} - A^*_{\theta\theta_0}(x)(x + u_0^*)^{-\frac{2}{3}}(x + u_{0j})^{-\frac{1}{3}}\Big).$$

The spatial integral can be written as

$$\hat{I}(u_{0j}, t_j) = \hat{I}_1(u_{0j}, t_j) - \hat{I}_2(u_{0j}, t_j) + \hat{I}_3(u_{0j}, t_j),$$

where

$$\hat{I}_i(u_{0j}, t_j) = \int_0^X I_i(u_0, x, t_j)dx, \qquad i = 1, 2, 3.$$

A quadrature in x is introduced via the weightings α_L to give,

$$\hat{I}_1(u_{0j}, t_j) = e^{-t_j} \sum_{L=1}^{m} \alpha_L (x_L + u_{0j})^{-\frac{7}{3}} \sum_{k=1}^{j} \alpha_k e^{\hat{t}_k}(x_L + u_{0k})^{\frac{4}{3}},$$

$$\hat{I}_2(u_{0j}, t_j) = e^{-t_j} \sum_{L=1}^{m} \alpha_L (x_L + u_{0j})^{-\frac{1}{3}} \sum_{k=1}^{j} \alpha_k e^{\hat{t}_k}(x_L + u_{0k})^{-\frac{2}{3}},$$

and

$$\hat{I}_3(u_{0j}, t_j) = e^{t^*-t_j} \sum_{L=1}^{m} \alpha_L A^*_{rr_0}(x)(x_L + u_{0j})^{-\frac{7}{3}}(x_L + u_0^*)^{\frac{4}{3}} - e^{t^*-t_j} \sum_{L=1}^{m} \alpha_L A^*_{\theta\theta_0}(x)(x_L + u_{0j})^{-\frac{1}{3}}(x_L + u_0^*)^{-\frac{2}{3}}.$$

An Euler iterative scheme is then used to integrate in time this non-linear system of ODEs to give

$$u_{0j+1} = u_{0j} + \delta t \frac{3u_{0j}}{4X}(X + u_{0j})\left(De\frac{A + Bu_{0j} + \Phi X}{u_{0j} + \Phi X} - P_u De - \frac{1}{\Gamma(u_{0j})^{\frac{1}{3}}} + \frac{2}{3}\gamma\hat{I}(u_{0j}, t_j)\right), \tag{4.10}$$

with initial conditions $u_0(t^*) = u_0^*$, $A_{rr_0}(x, t^*) = A^*_{rr_0}(x)$ and $A_{\theta\theta_0}(x, t^*) = A^*_{\theta\theta_0}(x)$ defined through matching this numerical solution with the inner solution. Note that for $t \gg 1$, the bubble volume found numerically through Eq. (4.10) is found to match with the equilibrium bubble volume u_∞, as defined by [16] and discussed following Eq. (2.24). Furthermore, for $t \gg 1$ it can be shown that $\hat{I} \to 0$, and as the bubble approaches its equilibrium volume $u_{0j+1} \to u_{0j}$. Setting $P_u = 0$ in Eq. (4.10) then recovers $DeP_{g_0} - 1/\Gamma {u_0}^{1/3} \to 0$ for $t \gg 1$, which corresponds to leading order with the limit stated in [16] for cases where the bubble growth rate is dominated by the surface tension towards the end of the bubble expansion.

The initial time t^* is selected as the boundary time at which the matched asymptotic solution transitions from the inner to the outer temporal region. This boundary time is defined as the time at

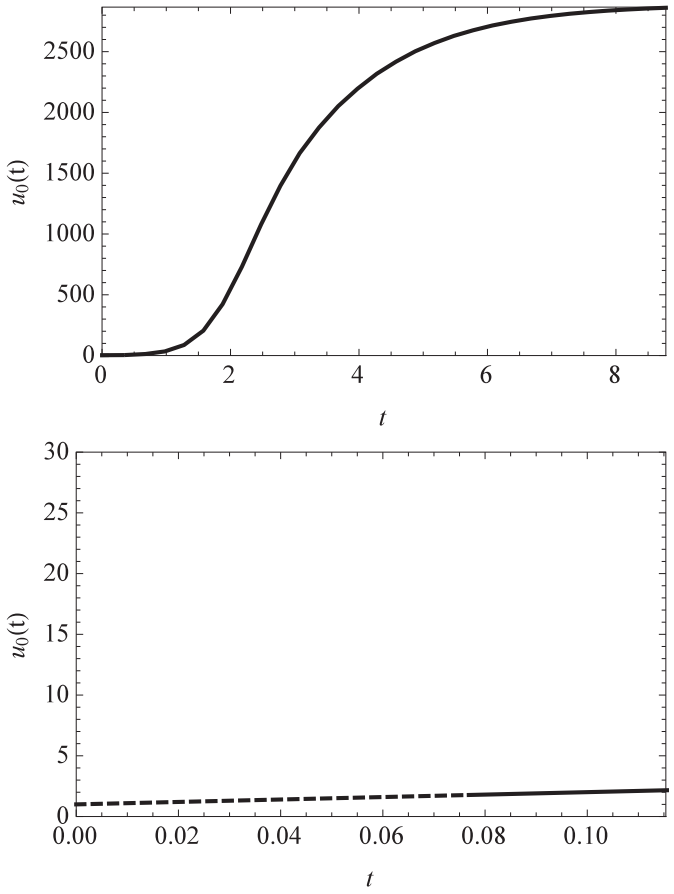

Fig. 6. (a) The first order inner solution given by Eq. (3.28) (dashed line) and the outer solution calculated through the Euler iterative scheme given by Eq. (4.10) (full line). The inner and outer solutions have been matched by selecting the time t^* such that the derivatives calculated from each respective equation are equal at this time, and the subsequent value of $u_0^\circ = u_0(t^*)$ initialises the Euler iterations. Plot (b) displays the same solutions, focused around t^* for clarity. The parameters common to both plots are as follows: $t^* = 0.077$, $X = 1000$, $p_a = 10^5$, $p_{g_o} = 10p_a$, $\Phi = 0.32$, $\Gamma = 1000$, $\gamma = 1$, $P_u = 0$ and $De = 9$.

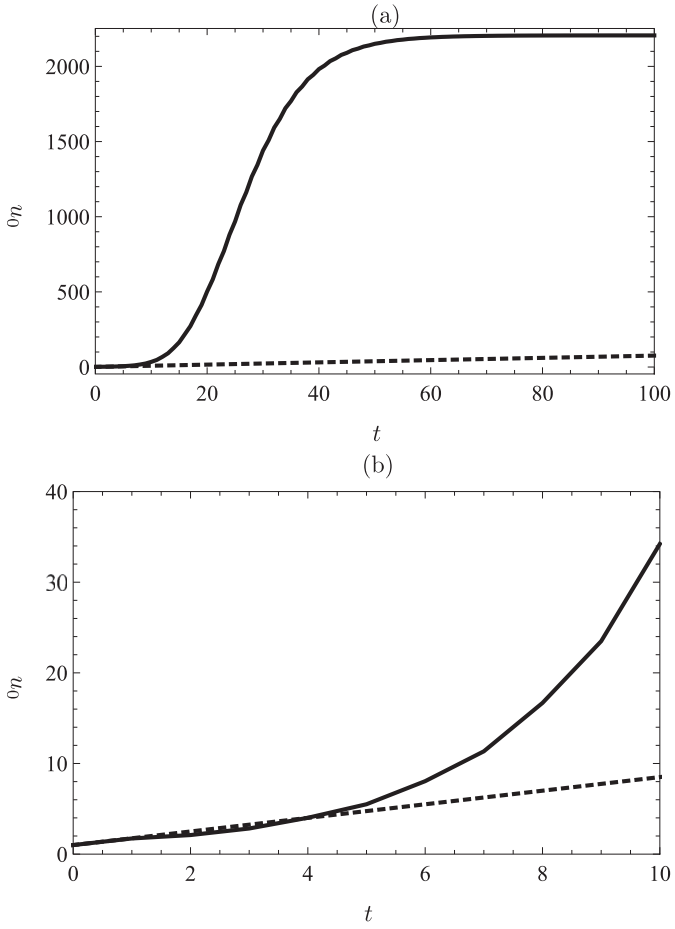

Fig. 7. (a) The first iterate, u_0^{p1}, for the analytic Picard solution (dotted line) given by Eq. (4.9) and the associated numerical solution calculated using the Euler iterative scheme given by Eq. (4.10) (solid line). Plot (b) shows that this first iterate is only reasonably accurate close to the initial condition at $t^* = 0$ and does not provide a good description of u_0 for $t \gg t^*$. The initial conditions and parameters common to both plots are as follows: $t^* = 0$, $u^* = 1$, $X = 1000$, $p_a = 10^5$, $p_{g_o} = 10p_a$, $\Phi = 0.32$, $\Gamma = 1000$, $\gamma = 1$, $P_u = 0$ and $De = 1$.

which the inner and outer solutions are equivalent; an additional requirement imposed here is that the gradients of the inner and outer solutions are equivalent at this boundary time, in order to ensure a smooth transition between the two regions. The boundary time t^* (the initial time of the outer solution scheme) can therefore be determined analytically by solving $0 = d/d\vartheta\,(U(t^*/\eta)) - d/dt(u_0(t^*))$ for t^* subject to $U(t^*/\eta)) = u_0(t^*) = u_{0_1}$, where $U(\vartheta)$ is defined by Eq. (3.28), $u_{0_{j+1}}$ is defined by Eq. (4.10), and the derivative of the discrete numerical iteration scheme (4.10) is defined as $d/dt(u_0(t_j)) = (u_{0_{j+1}} - u_{0_j})/\delta_t$. The initial volume u_0^* then initialises the Euler iteration (4.10), and the remaining initial conditions, $A^*_{rr_0}(x)$ and $A^*_{\theta\theta_0}(x)$, then follow directly. This matching is demonstrated in Fig. 6. In the limit as t gets very large, the bubble volume is shown to approach an asymptotic limit, and the value of this limit corresponds with the equilibrium bubble volume given in [16]. For the purpose of constructing Figs. 6–8 the Composite Simpson rule is used with quadrature weightings,

$$\alpha_1 = \alpha_m = \frac{h}{3}, \qquad \alpha_j = \begin{cases} \frac{4}{3}h, & j \text{ even} \\ \frac{2}{3}h, & j \text{ odd} \end{cases},$$

where $h = \delta x, \delta t$ and the accuracy is $O(h^4)$. Fig. 7 compares the Picard iteration solution with this numerical approach.

4.2. Investigating the effects of viscosity and the acoustic pressure amplitude on the final bubble volume

In Fig. 8 the numerical approach is used to look at the effect of altering the viscosity via the dimensionless parameter, De, and the dimensionless applied acoustic pressure amplitude, P_u. In the case of instantaneous diffusion, Fig. 8 (a) shows that an increase in P_u results in a decrease in the final bubble volume, though the time to achieve this steady state solution is unaffected. Note that by setting the inertia term to zero, the case of zero ultrasound pressure amplitude shown in Fig. 8 (a) is representative of the model presented in [16]. In Fig. 8 (b) the converse effect is evident due to increasing viscosity; that is, the steady state bubble volume is unaffected but the time required to reach this steady state volume is increased.

5. Conclusions and further work

A model has been produced to track the growth of a bubble in a free rising, non-reacting polymer foam incorporating the effects of inertia. The system was partially decoupled by assuming instantaneous diffusion, enabling inner and outer asymptotic solutions to be derived to first and leading order, respectively.

The asymptotic analysis performed in Section 3 derived an inner solution for the nondimensional bubble volume in the case

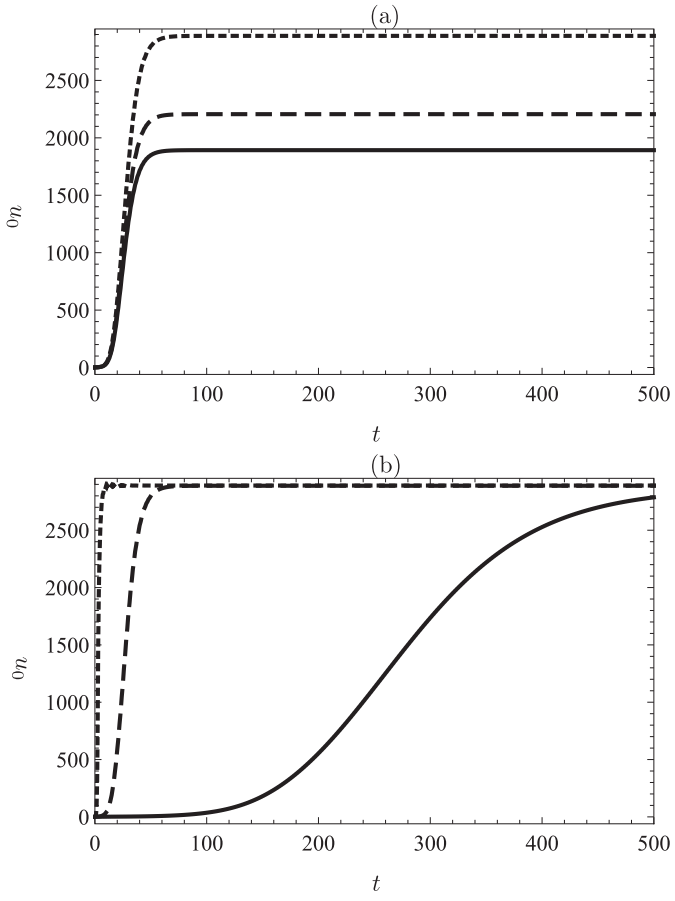

Fig. 8. The numerical solution of (4.10) and how it is affected by (a) acoustic pressure amplitude, P_u, and (b) viscosity via the dimensionless grouped parameter *De*. In (a) the values of P_u are zero (dotted line), 0.03 (dashed line) and 0.05 (solid line). The Deborah numbers, *De*, in (b) are 0.1 (solid line), 1.0 (dashed line) and 10.0 (dotted line), corresponding to viscosity values of 9×10^6 Nsm^{-2}, 9×10^5 Nsm^{-2} and 9×10^4 Nsm^{-2}, respectively. The initial conditions and parameters common to both plots are as described in Fig. 7 except for those parameter values detailed above for (a) and (b). Note that these $P_u = 0.03$ and $P_u = 0.05$ relate to acoustic pressure amplitude values of $p_u = 2.7 \times 10^4$ Pa and 4.5×10^4 Pa, respectively, and reflect instrumental values. In practice, the actual pressure amplitude, *in situ* would be much lower due to the effects of attenuation [43].

when the ratio of the bubble volume to the surrounding fluid volume is very small. This describes the non-reacting foam at early time when the bubbles have just nucleated and individual bubbles are located at large distances from neighbouring bubbles. The leading order solution was parameterised by the initial condition only and described the relationship between bubble volume and time as $U \propto t^{6/5}$.

In Section 4.2, increasing fluid viscosity is shown to have no impact on the final bubble volume; however, the time required to reach this equilibrium state is found to increase with the viscosity. This effect was also described by Everitt et al. [16]. They demonstrated two distinct phases of bubble growth in the case of instantaneous diffusion: an initial phase of rapid expansion in bubble volume followed by a second phase of slower expansion. The early time bubble growth displayed in Fig. 8 (b) agrees qualitatively with the results reported by Everitt et al. [16] for their numerical solution at early time. Critically, however, by including inertia in the work presented here, this paper has shown that inertia plays a substantial role in this phase of growth.

This paper was motivated by a problem regarding the tailoring of the porosity gradients within a cured sample of a polymerising foam under the influence of an acoustic standing wave [43].

Table 1
Parameters required for bubble expansion in the non-reacting system (2.19)–(2.23).

Parameter	Value	Units
Pressure outside the fluid layer, p_a	1	10^5Nm^{-2}
Initial bubble gas pressure, p_{g0}	10	10^5Nm^{-2}
Elastic modulus, G	1 – 10	10^5Nm^{-2}
Solvent viscosity, μ	1,6	10^5Nsm^{-2}
Polymer relaxation time, τ	1	s
Initial bubble volume, u_0	1	10^{-18}m^3
Surface tension, S	0 – 5	10^{-1}Nm^{-1}
Gas constant, R_g	8.31	Jmol^{-1}K^{-1}
Temperature, T	370	K
Henry's law constant, H	10.5	10^{-5}molN^{-1}m^{-1}
Diffusivity, D	0.1 – 100	10^{-12}m^{2}s^{-1}
Fluid density, ρ	1200	kgm^{-3}

This complex process involves many interacting factors and effects including rectified diffusion, Ostwald ripening and nucleation, all of which are affected by the variations in pressure amplitude resulting from the acoustic standing wave. While the acoustic pressure amplitude is found to have little impact on the early stages of bubble growth, Section 4.2 demonstrates that increasing the acoustic pressure amplitude results in a decrease in the final bubble volume. This promising result indicates that further investigations should be carried out to further explore the effects of the ultrasound field.

As has been demonstrated, the inertial effects are important in the early growth stages of the bubble. This would also be true in situations where the bubble was undergoing rapid oscillations due to an oscillating ultrasound field that was designed to cause the bubble to resonate. This resonating behaviour could affect the bubble growth via rectified diffusion. Only the time averaged RMS signal for the acoustic wave is considered in this paper, however, the scheme produced here could be employed in the future to examine the effects of the acoustic pressure amplitude on rectified diffusion.

The effect of the acoustic pressure amplitude of the irradiating standing wave will also have an effect on the bubble size distribution within an expanding polymer foam. Torres-Sanchez and Corney [43] observed that the porosity value at a given spatial point is directly proportional to the pressure amplitude at that point. The porosity value is related to bubble volume and future work will develop a mathematical model capable of tracking the bubble growth of a homogeneous distribution of bubbles under the influence of an acoustic standing wave. This will enable the relationship between porosity (or bubble size) and acoustic pressure amplitude which was observed by Torres-Sanchez and Corney [43] to be demonstrated mathematically (Table 1).

The ability to tailor the porosity profiles within polymerising materials will lead to significant improvements in a range of manufactured products such as artificial bone. Given the complexity of the physics involved it is essential that mathematical modelling underpins the design and implementation of the manufacturing process. This paper serves as the first stage in developing such a mathematical model and will pave the way in fully understanding this fascinating problem. The next steps will be to incorporate a reacting polymer into the framework presented here, and this will be addressed in future work.

Acknowledgements

This work was supported by the Engineering and Physical Sciences Research Council, grant reference EP/I033424/1.

Appendix A. Parameter values for numerical investigations

References

[1] M. Abramowitz, I. Stegun, Chapter 15: Hypergeometric functions, Handbook of Mathematical Functions: With Formulas, Graphs, and Mathematical Tables, Dover, New York, 1964.
[2] A. Adamson, A Textbook of Physical Chemistry, 2nd Ed. Academic Press, Inc., London, 2012.
[3] I. Akhatov, R. Mettin, C. Ohl, U. Parlitz, W. Lauterborn, Bjerknes force threshold for stable single bubble sonoluminescence, Phys. Rev. E 55 (3) (1997) 3747–3750.
[4] M. Amon, C. Denson, A study of the dynamics of foam growth: analysis of the growth of closely spaced spherical bubbles, Polym. Eng. Sci. 24 (13) (1984) 1026–1034.
[5] A. Arefmanesh, S. Advani, Diffusion-induced growth of a gas bubble in a viscoelastic fluid, Rheol. Acta 30 (1991) 274–283.
[6] N. Aziz, Bone Grafts and Bone Substitutes: Basic Science and Clinical Applications, World Scientific Publishing Co. Pte. Ltd., London, 2005.
[7] N. Bali, N. Iyengar, A Textbook of Engineering Mathematics, Laxmi Publications, New Delhi, 2004.
[8] S. Bose, M. Roy, A. Bandyopadhyay, Recent advances in bone tissue engineering scaffolds, Trends Biotechnol. 30 (10) (2012) 546–554.
[9] S. Cai, J. Xi, A control approach for pore size distribution in the bone scaffold based on the hexahedral mesh refinement, Comput. Aided Des. 40 (2008) 1040–1050.
[10] L. Crum, Measurements of the growth of air bubbles by rectified diffusion, J. Acoust. Soc. Am. 68 (1) (1980) 203–211.
[11] L. Crum, Rectified diffusion, Ultrasonics 22 (1984) 215–223.
[12] A. Eller, Effects of diffusion on gaseous cavitation in bubbles, J. Acoust. Soc. Am. 57 (6) (1975) 1374–1378.
[13] A. Eller, H. Flynn, Rectified diffusion during nonlinear pulsations of cavitation bubbles, J. Acoust. Soc. Am. 37 (3) (1965) 493–503.
[14] S. Everitt, O. Harlen, H. Wilson, Bubble growth in a two-dimensional viscoelastic foam, J. Nonnewton Fluid Mech. 137 (1–3) (2006a) 46–59.
[15] S. Everitt, O. Harlen, H. Wilson, Competition and interaction of polydisperse bubbles in polymer foams, J. Nonnewton Fluid Mech. 137 (1–3) (2006b) 60–71.
[16] S. Everitt, O. Harlen, H. Wilson, D. Read, Bubble dynamics in viscoelastic fluids with application to reacting and non-reacting polymer foams, J. Nonnewton Fluid Mech. 114 (2003) 83–107.
[17] M. Favelukis, Dynamics of foam growth: bubble growth in a limited amount of liquid, Polym. Eng. Sci. 44 (10) (2004) 1900–1906.
[18] J. Feng, C. Bertelo, Prediction of bubble growth and size distribution in polymer foaming based on a heterogeneous nucleation model, J. Rheol. 48 (2) (2004) 439–462.
[19] H. Fogler, J. Goddard, Oscillations of a gas bubble in viscoelastic liquids subject to acoustic and impulsive pressure variations, J. Appl. Phys. 42 (1) (1971) 259–263.
[20] D.W. Hutmacher, Scaffolds in tissue engineering bone and cartilage, Biomaterials 21 (24) (2000) 2529–2543.
[21] D. Kay, Schaum's Outline of Tensor Calculus, McGraw Hill Professional, New York, 1998.
[22] Y. Kojima, S. Koda, H. Nomura, Effect of ultrasonic frequency on polymerization of styrene under sonication, Ultrason. Sonochem. 8 (2001) 75–79.
[23] T. Leighton, Bubble population phenomena in acoustic cavitation, Ultrason. Sonochem. 2 (2) (1995) S123–S136.
[24] T. Leong, S. Wu, S. Kentish, M. Ashokkumar, Growth of bubbles by rectified diffusion in aqueous surfactant solutions, J. Phys. Chem. C 114 (2010) 20141–20145.
[25] P. Lewin, L. Bjorno, Acoustic pressure amplitude thresholds for rectified diffusion in gaseous microbubbles in biological tissue, J. Acoust. Soc. Am. 69 (3) (1981) 846–852.
[26] O. Louisnard, F. Gomez, Growth by rectified diffusion of strongly acoustically forced gas bubbles in nearly saturated liquids, Phys. Rev. E 67 (2003). 036610 (12pp).
[27] A. Markworth, Comments on foam stability, ostwald ripening, and grain growth, J. Colloid Interface Sci. 107 (2) (1985) 569–571.
[28] E. Mora, L. Artavia, C. Macosko, Modulus development during reactive urethane foaming, J. Rheol. 35 (5) (1991) 921–940.
[29] A. Naji Meidani, M. Hasan, Mathematical and physical modelling of bubble growth due to ultrasound, Appl. Math Model. 28 (2004) 333–351.
[30] D. Niyogi, R. Kumar, K. Gandhi, Modeling of bubble-size distribution in free rise polyurethane foams, AlChE J. 38 (8) (1992) 1170–1184.
[31] A. Polyanin, V. Zaitsev, Handbook of Exact Solutions for Ordinary Differential Equations, Chapman & Hall, London, 2003.
[32] G. Price, E. Lenz, C. Ansell, The effect of high intensity ultrasound on the synthesis of some polyurethanes, Eur. Polym. J. 38 (2002) 1531–1536.
[33] A. Prosperetti, Bubble phenomena in sound fields: part one, Ultrasonics 22 (2) (1984a) 69–77.
[34] A. Prosperetti, Bubble phenomena in sound fields: part two, Ultrasonics 22 (2) (1984b) 115–124.
[35] J. Schmelzer, F. Schwietzer, Ostwald ripening of bubbles in liquid-gas solutions, J. Non-Equilib. Thermodyn. 12 (1987) 255–270.
[36] M. Shafi, R. Flumerfelt, Initial bubble growth in polymer foam processes, Chem. Eng. Sci. 52 (4) (1997) 627–633.
[37] M. Shafi, K. Joshi, R. Flumerfelt, Bubble size distributions in freely expanded polymer foams, Chem. Eng. Sci. 52 (4) (1997) 635–644.
[38] C. Stewart, Nucleation and growth of bubbles in elastomers, J. Polym. Sci. 8 (1970) 937–955.
[39] J. Street, A. Fricke, L. Reiss, Dynamics of phase growth in viscous non-newtonian liquids, Ind. Eng. Chem. Fundam. 10 (1) (1971) 54–64.
[40] H. Tai, M. Mather, D. Howard, W. Wang, L. White, J. Crowe, et al., Control of pore size and structure of tissue engineering scaffolds produced by supercritical fluid processing, Eur. Cells Mater. 14 (2007) 64–77.
[41] Y. Ting, Viscoelastic effect of polymers on single bubble dynamics, AlChE J. 21 (4) (1975) 810–813.
[42] C. Torres-Sanchez, J. Corney, Identification of formation stages in a polymeric foam customised by sonication via electrical resistivity measurements, J. Polym. Res. 16 (2009b) 461–470.
[43] C. Torres-Sanchez, J. Corney, Porosity tailoring mechanisms in sonicated polymeric foams, Smart Mater. Struct. 18 (10) (2009a). 104001 (13pp).
[44] D.C. Venerus, Diffusion-induced bubble growth in viscous liquids of finite and infinite extent, Polym. Eng. Sci. 41 (8) (2001) 1390–1398.
[45] D.C. Venerus, N. Yala, B. Bernstein, Analysis of diffusion-induced bubble growth in viscoelastic liquids, J. Nonnewton Fluid Mech. 75 (1998) 55–75.
[46] Wilson, H.J.. Graduate Lectures: Polymeric Fluids. http://www.ucl.ac.uk/~ucahhwi/GM05; Accessed 2016.
[47] H. Winter, M. Mours, Rheology of polymers near liquid-solid transitions, Adv. Polym. Sci. 134 (1997) 165–234.
[48] T. Woodfield, J. Malda, Design of porous scaffolds for cartilage tissue engineering using a three-dimensional fiber-deposition technique, Biomaterials 25 (2004) 4149–4161.
[49] P. Yue, J. Feng, C. Bertelo, H. Hu, An arbitrary lagrangian-eulerian method for simulating bubble growth in polymer foaming, J. Comput. Phys. 226 (2007) 2229–2249.
[50] W. Zhai, J. Yu, J. He, Ultrasonic irradiation enhanced cell nucleation: an effective approach to microcellular foams of both high cell density and expansion ratio, Polymer 49 (2008) 2430–2434.